Systems/Circuits

Nasal Respiration Entrains Human Limbic Oscillations and Modulates Cognitive Function

Christina Zelano,[1] Heidi Jiang,[1] Guangyu Zhou,[1] Nikita Arora,[1] Stephan Schuele,[1] Joshua Rosenow,[2] and Jay A. Gottfried[1,3]

Departments of [1]Neurology and [2]Neurosurgery, Feinberg School of Medicine, Northwestern University, Chicago, Illinois 60611, and [3]Department of Psychology, Weinberg College of Arts and Sciences, Northwestern University, Evanston, Illinois 60208

The need to breathe links the mammalian olfactory system inextricably to the respiratory rhythms that draw air through the nose. In rodents and other small animals, slow oscillations of local field potential activity are driven at the rate of breathing (~2–12 Hz) in olfactory bulb and cortex, and faster oscillatory bursts are coupled to specific phases of the respiratory cycle. These dynamic rhythms are thought to regulate cortical excitability and coordinate network interactions, helping to shape olfactory coding, memory, and behavior. However, while respiratory oscillations are a ubiquitous hallmark of olfactory system function in animals, direct evidence for such patterns is lacking in humans. In this study, we acquired intracranial EEG data from rare patients (Ps) with medically refractory epilepsy, enabling us to test the hypothesis that cortical oscillatory activity would be entrained to the human respiratory cycle, albeit at the much slower rhythm of ~0.16–0.33 Hz. Our results reveal that natural breathing synchronizes electrical activity in human piriform (olfactory) cortex, as well as in limbic-related brain areas, including amygdala and hippocampus. Notably, oscillatory power peaked during inspiration and dissipated when breathing was diverted from nose to mouth. Parallel behavioral experiments showed that breathing phase enhances fear discrimination and memory retrieval. Our findings provide a unique framework for understanding the pivotal role of nasal breathing in coordinating neuronal oscillations to support stimulus processing and behavior.

Key words: **amygdala; hippocampus; local field potential; piriform cortex; respiration; respiratory oscillations**

Significance Statement

Animal studies have long shown that olfactory oscillatory activity emerges in line with the natural rhythm of breathing, even in the absence of an odor stimulus. Whether the breathing cycle induces cortical oscillations in the human brain is poorly understood. In this study, we collected intracranial EEG data from rare patients with medically intractable epilepsy, and found evidence for respiratory entrainment of local field potential activity in human piriform cortex, amygdala, and hippocampus. These effects diminished when breathing was diverted to the mouth, highlighting the importance of nasal airflow for generating respiratory oscillations. Finally, behavioral data in healthy subjects suggest that breathing phase systematically influences cognitive tasks related to amygdala and hippocampal functions.

Introduction

The act of breathing results in a cyclical flow of air through the nose, providing an entry point for respiratory entrainment of neural activity. In mammals, local field potential (LFP) responses in olfactory bulb and piriform cortex (PC) oscillate in phase with breathing (Adrian, 1942; Kay and Freeman, 1998; Fontanini et al., 2003), and when breathing is diverted away from the nose, these patterns diminish (Fontanini et al., 2003). Based on such findings, it has been proposed that dynamic oscillatory rhythms regulate cortical excitability, synchronize activity within cell assemblies, and coordinate network interactions, helping to shape olfactory sensory coding, memory, and behavior (Laurent et al., 2001; Kay, 2005; Kepecs et al., 2006; Martin and Ravel, 2014).

Breathing is a vital rhythm of mammalian life, replenishing the bloodstream with oxygen and eliminating carbon dioxide with essential regularity. Although the respiratory drive is generated by conditional bursting pacemaker neurons in the brainstem (Smith et al., 1991, 2009; Garcia et al., 2011), its pace is not fixed:

Received Aug. 14, 2016; revised Sept. 24, 2016; accepted Oct. 12, 2016.

Author contributions: C.Z. and J.A.G. designed research; C.Z., H.J., N.A., S.S., J.R., and J.A.G. performed research; C.Z., H.J., and G.Z. analyzed data; C.Z. and J.A.G. wrote the paper.

This work was funded by National Institutes of Health Grants R00-DC-012803 (to C.Z.), and R21-DC-012014 and R01-DC-013243 (to J.A.G.), and a National Science Foundation Graduate Research Fellowship Program grant (to H.J.). We thank Enelsa Lopez, Jeremy Eagles, and all of the clinical staff in the Comprehensive Epilepsy Center at Northwestern Memorial Hospital for their invaluable help with technical aspects of intracranial EEG data collection. We also thank Thorsten Kahnt and Marc Slutzky for their comments on the manuscript.

The authors declare no competing financial interests.

Correspondence should be addressed to Christina Zelano, Department of Neurology, Northwestern University, Feinberg School of Medicine, Chicago, IL 60611. E-mail: c-zelano@northwestern.edu.

DOI:10.1523/JNEUROSCI.2586-16.2016

 0270-6474/16/3612448-20$15.00/0

a variety of emotional and cognitive states, including anxiety (Boiten, 1998), stress (Suess et al., 1980), and exploratory behavior (Welker, 1964; Kay and Freeman, 1998; Verhagen et al., 2007; Evans et al., 2009; Vlemincx et al., 2011; Huijbers et al., 2014), can all modify the rate and depth of breathing. The alternative idea, that respiratory phase exerts a direct impact on emotion and cognition, is unknown. The fact that the olfactory system is closely linked with limbic brain regions mediating emotion, memory, and behavior (Carmichael et al., 1994; LeDoux, 2000; Eichenbaum et al., 2007) suggests a robust pathway by which nasal breathing could even shape rhythmic electrical activity in downstream limbic areas, with corresponding effects on cognitive functions.

In line with these ideas, the power of fast cortical oscillations can be modulated by rhythmic external events occurring at lower frequency (Lakatos et al., 2005), with recent animal work revealing that breathing entrains high-frequency oscillations in both olfactory brain regions (Rojas-Líbano et al., 2014; Frederick et al., 2016) and nonolfactory areas, including whisker barrel cortex (Moore et al., 2013; Ito et al., 2014) and hippocampus (Yanovsky et al., 2014; Nguyen Chi et al., 2016). Interestingly, new behavioral data in rodents show that sniffing can even impact nonolfactory behaviors, such as whisking (Cao et al., 2012; Ranade et al., 2013) and ultrasonic vocalizations (Sirotin et al., 2014). Thus, data across a wide range of studies and sensory modalities suggest that respiratory rhythms modulate oscillatory patterns throughout the brain, with potential impact on stimulus sampling behaviors. One broad implication is that breathing subserves more than just supplying oxygen to the body; it can also organize neuronal population activity across brain regions to orchestrate complex behaviors affiliated with orofacial sensation (Kleinfeld et al., 2014). Whether respiratory rhythms have a direct influence on cortical oscillations in the human brain is not well understood.

Here we used intracranial EEG (iEEG) methods to test four inter-related hypotheses about breathing, the brain, and cognition. First, we asked whether respiratory-induced oscillations are present in human PC. Such evidence has been elusive, given that surface EEG approaches lack the spatial resolution and functional MRI (fMRI) approaches lack the temporal resolution to identify oscillatory activity in deeply situated olfactory structures. Second, we asked whether respiratory oscillations propagate to amygdala and hippocampus, and, if so, whether these depend on airflow stimulation through the nose. This question was designed to establish a mechanistic basis for our third hypothesis, examining whether breathing phase systematically influences cognitive tasks related to amygdala and hippocampal functions. Finally, in one patient, we directly tested the idea that respiratory oscillations in the amygdala influence performance on an emotion judgment task, which would imply that the breathing rhythm can exert potent control over learning and behavior.

Materials and Methods

Study participants. Participants in the iEEG experiment included seven patients (three women) with temporal lobe epilepsy whose seizures were poorly controlled by medication (Table 1, demographic and clinical details). An eighth patient was specifically recruited to participate in the emotion judgment task (Table 1, patient P8 details). Patients were recruited for the study only if the planned clinical electrode coverage provided coverage of PC, amygdala, and/or hippocampus. Behavioral study participants included a total of 107 healthy human subjects between the ages of 18 and 30 years. All participants gave informed consent to take part in the study, and all experiments were approved by the Institutional Review Board of Northwestern University. During iEEG data acquisition, patients were asked to sit quietly, breathing naturally for 15 min. They were asked to keep their eyes open, and one member from the research team sat in the room with the patient during this time. If patients became fatigued or the task was interrupted, the experiment was stopped and resumed later.

Electrophysiology. iEEG data were recorded using a clinical Nihon Kohden system in place at Northwestern Memorial Hospital (NMH). The Nihon Kohden recording system allows sampling frequency of up to 2000 Hz, and can reliably handle high-pass filters from 0.08 Hz, thus allowing the recording of very low-frequency oscillations, well below the range of natural breathing in humans. The system also allows four DC input channels. Our data were recorded with a sampling rate of 1000 Hz. Reference and ground were obtained from a surgically implanted electrode strip that was placed specifically for this purpose, facing away from the brain (toward the scalp). All data were rereferenced to a common average before further data analysis. Our rationale for using a common average reference was based on the fact that this reference could be used in all of the patients, ensuring consistency of methods across patients. Depending on clinical needs and surgical approach, electrode coverage varied across patients. This meant that it was difficult to find an appropriate single reference electrode that was in a similar location across patients.

Electrode locations did not deviate from standard clinical coverage for medial temporal epilepsy patients at NMH, and included four depth electrodes, implanted along an oblique coronal plane and (across the four electrodes) intended to span the long axis of the medial temporal lobe. As standard clinical procedure at NMH, respiration was recorded using a piezoelectric pressure sensor attached to a nasal cannula at the patient's nose (Salter Labs), and breathing belts placed around the abdomen (see Respiratory physiological recordings and analysis, for additional information). The electrodes used to record LFP data for this study were eight-contact depth electrodes (Integra Epilepsy, Integra) using the Leksell frame and Brainlab planning system (iPlan Stereotaxy version 3.0, Brainlab). Electrodes had 5 mm center-to-center spacing between adjacent electrode contacts. Data were recorded in separate blocks of ~15 min in length, corresponding to the behavioral tasks performed. Preoperative structural MR images were acquired on all patients with a 1.5 T MRI scanner. Computed tomography (CT) scans were acquired postoperatively with subdural electrodes in place, clearly showing electrode positions with respect to skull geometry. CT scans were aligned to T1 images using the Oxford Centre for Functional MRI of the Brain Software Library (FSL5). Coregistered CT scans underwent visual inspection and manual translation was performed via MATLAB if major structural landmarks were still not properly aligned. Electrode localization was then performed on coregistered CT scans using CTMR implemented in MATLAB (Hermes et al., 2010).

Respiratory physiological recordings and analysis. Our method of measuring respiration varied depending on the task and the location of the experiment. Respiratory recording methods were as follows, for each task:

Intracranial EEG recordings in patients who underwent nasal breathing: pressure sensor (Salter Labs). As temporal resolution of the breathing signal was most critical for time locking of the iEEG experiments, this pressure sensor is the ideal choice for measuring the temporal dynamics of respiration (Johnson et al., 2006).

Intracranial EEG recordings in patients who underwent both nasal and oral breathing: abdominal breathing belt (Perfect Fit II Adult Effort Belt, DyMedix Diagnostics). Because the Salter Labs pressure sensor is unable to detect changes in oral breathing, we used an abdominal breathing belt, enabling us to compare nasal and oral breathing from the same patient using the same breathing device. Therefore, any differences in spectral power between nasal and oral breathing cannot be attributed to differences in the respiratory measurement technique.

Behavioral recordings in healthy subjects participating in the nasal breathing version of the emotion and memory tasks: pneumotachometer (4719 Series, 0–100 LPM, Hans Rudolph), which uses a flow head connected to a fine mesh stainless steel screen to generate a pressure signal proportional to the airflow rate. The response-time performance of this device has been found to be very similar to that of the pressure sensor (Johnson et al., 2006).

Table 1. Patient demographics

Patient	Description
P1	
Handedness	Left
Age at surgery	33 years
Seizure risk factors	Reye's syndrome with convulsions as a child
Family history of seizures	(+) Maternal grandfather
Age of seizure onset	25 years
Seizure semiology	Automotor seizures; generalized tonic-clonic
Working diagnosis	Nonlesional left temporal lobe epilepsy
EEG	Left temporal interictal discharges
MRI brain	Normal
Current medications	Lamotrigine, oxcarbazine, Vimpat, clorazepate
P2	
Handedness	Left
Age at surgery	47 years
Seizure risk factors	Head injury at age 3 with loss of consciousness, viral encephalopathy age 45 years
Family history of seizures	None
Age of seizure onset	45 years
Seizure semiology	Psychic aura, gustatory aura, complex partial seizure
Working diagnosis	Nonlesional left temporal lobe epilepsy
EEG	Bitemporal ictal discharges; interictal left temporal sharp waves
MRI brain	Normal
Current medications	Valproic acid, lamotrigine, phenytoin
P3	
Handedness	Right
Age at surgery	29 years
Seizure risk factors	None
Family history of seizures	None
Age of seizure onset	22 years
Seizure semiology	Generalized tonic-clonic seizures, dialeptic seizures, tonic seizures
Working diagnosis	Nonlesional left temporal lobe epilepsy
EEG	Left temporal spikes
MRI brain	Normal
Current medications	Topiramate, oxcarbazine, levetiracetam, lacosamide
P4	
Handedness	Right
Age at surgery	49 years
Seizure risk factors	Hodgkin's lymphoma age 17, splenectomy, stroke at age 48 years
Family history of seizures	(+) Niece
Age of seizure onset	23 years
Seizure semiology	Generalized tonic– clonic seizures, automotor seizures, postictal aphasia
Working diagnosis	Lesional left temporal lobe epilepsy
EEG	Left temporal sharp waves
MRI brain	Chronic stroke/encephalomalacia in left putamen, insula, parietal cortex
Current medications	Carbamazepine, lamotrigine, levetiracetam
P5	
Handedness	Right
Age at surgery	48 years
Seizure risk factors	Head trauma with loss of consciousness as a child
Family history of seizures	None
Age of seizure onset	37 years
Seizure semiology	Complex partial seizure
Working diagnosis	Nonlesional right temporal lobe epilepsy
EEG	Right temporal sharp waves
MRI brain	Few small T2 hyper-intense foci in frontal subcortical white matter
Current medications	Levetiracetam, lamotrigine, oxcarbazine, clonazepam
P6	
Handedness	Right
Age at surgery	57 years
Seizure risk factors	None
Family history of seizures	None
Age of seizure onset	12 years
Seizure semiology	Complex partial seizures with secondary generalization; ictal aphasia
Working diagnosis	Left temporal lobe epilepsy
EEG	Left posterior temporal sharp waves and seizures
MRI brain	Subtle right hippocampal volume loss
Current medications	Valproic acid, primidone, Vimpat
P7	
Handedness	Right
Age at surgery	34 years
Seizure risk factors	None
Family history of seizures	None
Age of seizure onset	24 years
Seizure semiology	Generalized convulsions; complex partial seizures; automotor seizures; aphasia
Working diagnosis	Left temporal lobe epilepsy
EEG	Left temporal slowing and seizures
MRI brain	Normal
Current medications	Lamotrigine, phenobarbital, Vimpat
P8	
Handedness	Right
Age at surgery	59 years
Seizure risk factors	None
Family history of seizures	None
Age of seizure onset	12 years
Seizure semiology	Psychic aura; automotor seizures; generalized tonic-clonic epilepsy
Working diagnosis	Temporal lope epilepsy
EEG	Left posterior temporal-parietal sharp waves
MRI brain	Subtle volume loss in right hippocampus
Current medications	Valproic acid, primidone, Topamax

Behavioral recordings in healthy subjects participating in the oral breathing version of the emotion and memory tasks: abdominal breathing belts (Siemens).

Behavioral recordings in healthy subjects participating in the control (nasal breathing with mouth open) version of the emotion and memory tasks: both pneumotachometer (4719 Series, Hans Rudolph) and abdominal breathing belt (RX-TSD221-MRI, Biopac Systems). This enabled us to directly compare the breathing belt data and the pneumotachometer data.

Respiratory data for iEEG experiments were recorded, digitized, and filtered (0–15 Hz) on-line through a DC input directly into the Nihon Kohden clinical EEG recording system. The main goal of off-line analysis of the breathing time-series data (in MATLAB) was to identify the time of peak inspiratory flow for each breath (trial) in the respiratory time series. As noted above, the pressure sensor is coupled to piezo pressure sensor technology to measure airflow pressure. Because this sensor is positioned at the nasal cannula, the device is effectively an "open" system (unlike the "closed" system of a bellows-type respiratory device that measures chest expansion and/or lung volume). This open system means that the device is most sensitive to changes in airflow. Thus, the most sensitive point of the respiratory signal occurs at the maximal inspiratory flow, precisely where the inflection point from an upward slope (accelerating phase of inspiration) to a downward slope (decelerating phase of inspiration) occurs. When the subject has completed an inhalation, but before beginning exhalation, the respiratory signal will begin to return to zero, since at

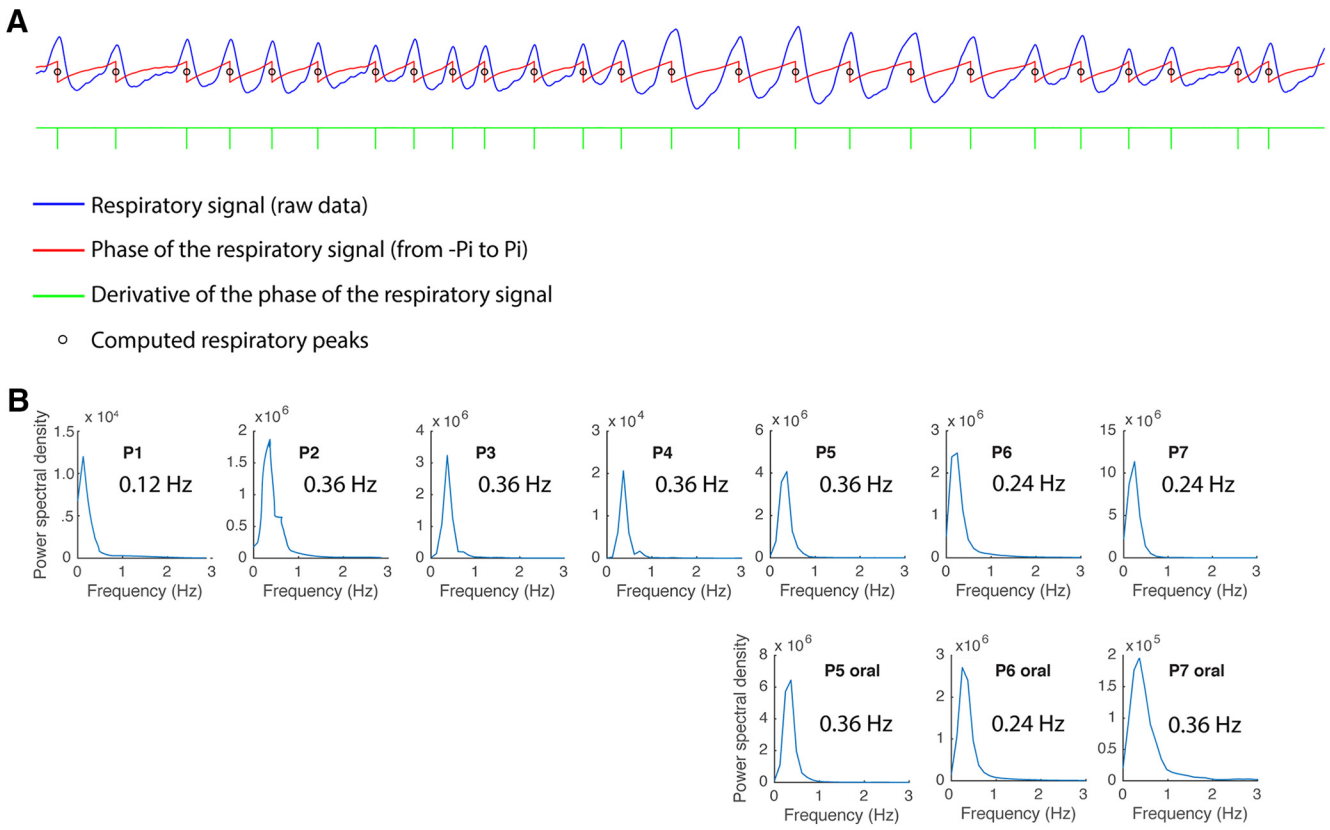

Figure 1. Respiratory analysis method and breathing frequency data across patients. ***A***, A representative trace of the raw respiratory signal from one patient is shown in blue. To define respiratory events for the LFP analyses, the instantaneous phase of the respiratory time series (obtained from the angle of the Hilbert transform) was computed (red trace). The peak of inspiratory flow occurs at the abrupt transition in the instantaneous phase from π to $-\pi$, and can be detected as a deflection in the derivative of the phase of the respiratory signal (green tick marks). The small black circles on the respiratory phase waveform (in red) denote the points of peak flow, which align well to the inspiratory peaks of the raw respiratory signal (in blue). ***B***, Fast Fourier transform analysis was used to characterize the dominant breathing frequency in each patient. Each panel represents one patient (P1–P7).

this point the flow of air has ceased. As a result of these temporal dynamics of the breathing signal, the component of the recorded breathing signal that is most reliably detected using automated MATLAB scripts is the inspiratory peak airflow.

To obtain reliable estimates of the time-points of peak inspiratory flow, we computed the instantaneous phase of the respiratory signal, using the Hilbert transform function in MATLAB (Fig. 1). In this way, the peak flow could be estimated as the abrupt discontinuity in phase, which could be easily identified by taking the derivative of the phase of the respiratory signal (Fig. 1*A*, green tick marks). Specifically, the respiratory signal was thresholded two times. First, the derivative of the phase was thresholded to identify sharp peaks corresponding to respiratory maximal flow. We then further thresholded the value of the physiological respiratory signal for each identified event to include only those that were >0.75 SD from the mean, to minimize contributions of signal noise. All trials were then manually inspected to ensure accuracy. While there are different methods to determine respiratory peaks, this method was robust to changes in the timing and amplitude, as well as to occasional noisy segments, of the breathing signal.

To characterize the rate of natural breathing in each patient, we performed a fast Fourier transform analysis in MATLAB ("pwelch" function; segment length, 8192 ms; 90% overlap; Hanning window length, 8192 ms). This approach confirmed that the dominant breathing frequency in most patients was 0.24–0.36 Hz, corresponding to 14.4–21.6 breaths/min (Fig. 1*B*).

LFP data preprocessing. Analyses of the LFP time-series data were performed using MATLAB (MathWorks) and a combination of EEGLAB code (Delorme and Makeig, 2004), FieldTrip code (Oostenveld et al., 2011), and in-house code. Interictal spikes were removed using an automated spike sorting algorithm (Yadav et al., 2011) and manual inspection of EEG time series. The data were analyzed both with and without spike removal, with similar results. The following sections provide specific details about LFP analyses of the slow respiratory oscillations, the higher-frequency spectral data, and the cross-frequency coupling (CFC).

LFP analysis of slow respiratory oscillations. To determine whether very low-frequency neural oscillations in the human respiratory range were coherent with respiration, we focused on the individual averaged LFP data in each patient separately. Data were analyzed from 15 min periods of wake during which the patient was resting quietly and breathing naturally through the nose, during times when the patients were undisturbed by visitors, including research and clinical staff. We used a low-pass filter (<0.6 Hz) for extracting the low-frequency LFP signal corresponding to the human respiratory range. This procedure also had the advantage of removing higher-frequency oscillatory effects that might be aligning to respiration. A two-pass least-square finite-impulse response (FIR) filter (order = three times the lower frequency bound) was used to prevent phase distortion. It is worth noting that because our recording system is only able to record at frequencies >0.08 Hz, this filtering effectively amounted to a bandpass filter of 0.08–0.6 Hz.

Filtering of the low-frequency signal was performed across the entire 15 min raw LFP time series, which was then divided into separate 6 s trials aligned to peak inspiratory flow for each respiratory trial (Figs. 2, 3). These 6 s windows were simply used as the time windows within which trials were binned, where peak flow was set to 0 s. As such, the −2 s time-point did not necessarily denote the onset of inspiration, nor did the +4 s time-point denote the end of the breath. Basically, the 6 s windows ensured that each breath trial was fully captured in that period of time; because patients often initiated a second breath within 6 s, we included only every other respiratory peak in the spectral analysis to eliminate data overlap across trials.

Respiratory and LFP trials (each of 6 s duration, aligned to peak inspiratory flow at 0 s) were then averaged, and the linear correlation was

computed and Fisher *z*-transformed. To assess statistical significance, the same procedure was followed, but using 6 s windows of LFP data that were aligned to random time points with regard to the peak flow onset times in the respiratory data (Fig. 3). This process was repeated 1000 times to generate a statistically null distribution of *R* values. Comparison of each patient's actual *R* value to their *R*-null distribution enabled us to derive a *p* value (such that an effect was significant if the actual value fell within the top 5% of the distribution).

LFP spectral analysis of higher-frequency oscillations. To determine whether respiratory phase entrains higher-frequency oscillations across limbic brain regions, we computed spectrograms in each region for each patient individually (Fig. 4*A–C*, left columns). Time–frequency decomposition of the neural time-series data was conducted using a filter-Hilbert approach, a widely accepted algorithm for analysis of EEG time series (Bruns, 2004; Canolty et al., 2006; Cohen, 2014; Szczepanski et al., 2014). First, we used a two-pass FIR filter (order = three times the lower frequency bound), to create 101 log-spaced frequency steps, with center frequencies ranging from 1 to 200 Hz, and with frequency bandwidths (window sizes) logarithmically increasing in 101 steps from 1 to 10 Hz. These procedures were applied to the entire 15 min raw LFP time series individually for each patient.

Next, the instantaneous amplitude at each time point and each frequency band was extracted using the element-wise modulus of the Hilbert transform, and then the resulting amplitude time series were segmented into 6 s epochs, centered at the peak inspiratory flow at 0 s. Spectrograms were then created by averaging across all trials, followed by temporal smoothing with a moving average window of 10 ms. As was done for the LFP analysis of slow respiratory oscillations, we used a 6 s window to ensure that at least one breath trial was fully captured in that period of time, and only entered every other respiratory peak into this analysis to minimize data overlap between breaths.

Finally, the spectrogram was normalized (per frequency) by subtracting the mean amplitude from 0.2 to 0.8 s (depicted as a thick black bar on the horizontal axis of all spectrograms (Figs. 4, 5, 6). The significance of amplitude changes was determined using a bootstrap method (Canolty et al., 2007). In brief, the actual inspiratory peaks were circularly shifted by a random amount while reserving the number of samples between successive trials. Surrogate mean amplitudes were obtained by averaging the amplitude of the surrogate indices. A distribution of surrogate values was obtained after repeating this procedure 10,000 times. The *z*-scored actual mean amplitude change was calculated by dividing the mean amplitude change by the SD of the surrogate ensample. The *z* maps were then thresholded for statistical significance using false discovery rate (FDR) correction for multiple comparisons (Benjamini and Hochberg, 1995). Frequency bands were defined as follows: delta band, 0.5–4 Hz; theta band, 4–8 Hz; alpha band, 8–13 Hz; beta band, 13–30 Hz; gamma band, 30–200 Hz.

Analysis of cross-frequency coupling. Phase-amplitude coupling was examined using the modulation index (MI), which is an estimate of the normalized entropy of the phase-amplitude distribution (Tort et al., 2008). Analysis of cross-frequency coupling between the low-frequency phase and higher-frequency amplitude involved three steps. The first step was designed to extract instantaneous phase data across a set of low frequencies between 1 and 10 Hz. To this end, a two-pass FIR filter (order = three times the lower frequency bound) was used to create 19 equally spaced frequency steps across the full 15 min LFP time series, with center frequencies ranging from 1 to 10 Hz, and with fixed-frequency bandwidths of 2 Hz. These parameters provided sufficient sensitivity to assess most of the lower end of the delta band. The instantaneous phase was then determined from the element-wise angle of the Hilbert-transformed signal for each of the 19 frequency steps.

The second step was designed to extract instantaneous amplitude data across a set of higher frequencies between 13 and 200 Hz. To this end, a two-pass FIR filter (order = three times the lower-frequency bound) was used to create 100 log-spaced frequency steps over the 15 min LFP time series, with center frequencies between 13 and 200 Hz, and with frequency bandwidths logarithmically increasing between 4 and 50 Hz. The instantaneous amplitude was then determined from the element-wise modulus of the Hilbert-transformed signal for each of the 100 frequency steps.

The final step involved computation of the MI. For each phase-amplitude combination, a histogram of amplitude values was generated using 20 phase bins. Following published methods (Tort et al., 2008), the entropy of each phase-amplitude histogram was computed to generate MI values for each combination. These values were then plotted onto a 2-D comodulogram (Fig. 7). To test the significance of the modulation index, 200 surrogate modulation indices that were calculated using a combined, randomly shifted phase and the amplitude time series were obtained (Canolty et al., 2006). The *z*-scored modulation index was obtained by subtracting the surrogate mean value from the actual modulation index, which was then divided by the SD of the surrogate distribution.

Emotion recognition task. A total of 70 healthy subjects between the ages of 18 and 30 years participated in this task: 24 subjects performed the task during nasal respiration (13 women), 18 subjects performed the task during oral respiration (12 women), and 28 subjects performed the task during nasal respiration with the mouth held open as an attentional control (18 women). In the nasal version of the task, 3 of the 24 nasal subjects were excluded (1 subject fell asleep during the task, 1 subject had nasal congestion resulting in difficulty breathing through the nose, and 1 subject had an excessive number of missed trials across the session), leaving a total of 21 subjects. In the oral version of the task, 1 of the 18 subjects was excluded because her nasal airway was not properly blocked, leaving a total of 17 subjects. In the attentional control task, 4 subjects were excluded (3 subjects due to technical problems with the respiratory recording equipment, and 1 subject had an excessive number of missed trials), leaving a total of 24 subjects. Thus, there was a total of 62 healthy subjects who completed these studies.

Before the start of the experiment, subjects were affixed with either a pneumotachometer positioned in front of the nostrils (nasal task) or with a pair of breathing belts placed around the abdomen (oral task). For subjects taking part in the oral version of the task, a small piece of tape was lightly placed across the nostrils to minimize nasal contributions to breathing. For subjects taking part in the attentional control task, a pneumotachometer and an abdominal breathing belt were both affixed. These subjects were asked to breathe through their nose while holding their mouths open.

The emotion task consisted of viewing a set of faces with either a fearful or surprised expression (see Fig. 8). The task was presented on a Macbook Pro using PsychToolbox (Brainard, 1997; Pelli, 1997) through MATLAB. On each trial, a stimulus was presented for 100 ms, with an intertrial interval (ITI) randomly jittered between 2 and 5 s (mean ITI, 3.5 s) to ensure that stimuli fully "tiled" all phases of the respiratory cycle. Upon viewing a face, subjects had to indicate by pushbutton as quickly and accurately as possible whether an expression of fear or surprise was present, using the buttons (buttons "1" and "2") on a computer keyboard. In total, 18 different faces were presented in each task, with each face repeated 10 times. There was a total of 180 emotion recognition trials occurring within a single session of 11 min. The intertrial interval reported (average, 3.5 s) was programmed to include the response time (RT). Thus, to record a response, participants were forced to respond within the ITI. This was because we aimed to have control over the time between when each stimulus was presented so as to minimize any systematic lag that could be generated if reaction times varied systematically with respiration. In addition to the emotion task, subjects also took part in a control gender discrimination task. In this instance, subjects viewed faces with either a happy or neutral expression. Task parameters were otherwise identical. The order of the emotion and gender tasks was counterbalanced across subjects. All stimuli came from the Ekman (1975) face set.

Condition-specific stimulus presentations (fear/surprise faces in the emotion task; male/female faces in the gender task) were synchronized with the respiratory trace recorded via PowerLab (ADInstruments). Subsequently, all trials were categorized by respiratory phase, determined by estimating the angle of the Hilbert transform of the respiratory signal. In the nasal condition, in which a spirometer was used to record breathing, trials were categorized as inspiratory trials when the stimulus occurred between $-\pi/2$ and $\pi/2$ of the respiratory phase, whereas trials were categorized as expiratory trials when the stimulus occurred between $-\pi$ and $-\pi/2$ or between $\pi/2$ and π of the respiratory phase. In the oral

condition, in which a breathing belt was used to record breathing, stimuli that landed within respiratory phases of $-\pi$ and 0 were categorized as inspiratory trials (because of differences in the nature of the breathing belt signal compared with the spirometer signal), and those that landed within respiratory phases of 0 and π were categorized as expiratory trials. At the level of individual subjects, the reaction time of each trial was square root transformed, and the mean was computed subsequently across the square root reaction times (within condition). Reaction times that were 3 SDs above or below the mean were excluded. Mean reaction times and accuracies were compiled for each subject and condition, and then submitted to group-level analysis. For reaction time analyses, incorrect responses were excluded. For group-level analyses, repeated-measures ANOVAs were performed comparing breathing route, emotion, and phase, followed by confirmatory ANOVAs and *t* tests.

By recording respiration both via pneumotachometer and breathing belt during the attentional control task (breathing through the nose with the mouth held open), we were able to directly compare behavioral results obtained from the two respiratory recording methods. We found that it made no difference whether the pneumotachometer or the breathing belt was used to classify fearful faces into the inspiratory or expiratory phase of breathing: with both techniques, fearful faces were detected significantly more quickly during inspiration than expiration, as evidenced by an ANOVA computed between measure (belt/pnuemotach) and phase (inhale/exhale). There remained an overall effect of phase ($F_{(1,23)} = 9.31$, $p = 0.005$), and no interaction between measure and phase ($F_{(1,23)} = 0.58$, $p = 0.45$), suggesting that the abdominal breathing belt provided adequate temporal resolution to resolve the behavioral trials according to the phase in which they appeared.

Visual object memory task. A total of 42 healthy subjects between the ages of 18 and 30 years took part in this task (Fig. 9), including 13 subjects (8 women) enrolled in the nasal version of the task, 13 subjects (9 women) enrolled in the oral version, and 16 subjects (8 women) enrolled in the control (nasal breathing/mouth open) version. One subject from the nasal condition was excluded because the pneumotachometer became detached during testing, and one subject from the oral condition was excluded because her nasal airway (at the nostrils) was not adequately blocked. Four subjects from the attentional nasal condition were excluded due to experimenter error (the wrong experimental task was administered). A further subject from each condition was excluded due to an excessive number of missed trials (>10%), leaving a total of 11 subjects in each condition. Stimuli consisted of objects of various human-made and organic categories (e.g., buildings, fruits, instruments), obtained from the set available from Moreno-Martínez and Montoro (2012). A total of 180 of these objects were randomly assigned to the encoding session. Stimuli were previously ranked in salience, enabling us to exclude stimuli within the top or bottom 15% of salience ratings.

Before the encoding session, subjects were told they would view images that they would later be asked to recall. During the encoding session (15 min duration), 180 stimuli were presented for 500 ms. The ITI was randomly jittered between 3 and 6 s (mean ITI, 4.5 s) to ensure that stimuli fully spanned all phases of the respiratory cycle. Following a 20 min break (during which time subjects performed the emotion and gender tasks), subjects took part in a memory retrieval session, consisting of the 180 "old" stimuli and 180 "new" stimuli. During memory retrieval, subjects were asked to indicate whether each image had been previously seen during initial encoding ("old") or had not been seen before ("new"). All stimulus presentation times in both sessions were recorded on-line using PowerLab (ADInstruments), in synchrony with recording of the respiratory signals. Data analysis was performed in MATLAB.

Respiratory phase during each stimulus was determined by estimating the circular mean of the instantaneous angle of the Hilbert transform of the breathing signal over the duration of stimulus presentation. Responses evoked by each object image during retrieval were categorized into the respiratory phase of either the actual phase of respiration at retrieval, or the phase of respiration during initial encoding. Respiratory phase was determined in the same way as described above in the emotion recognition task. Reaction times (square root transformed) were averaged, and accuracies were computed across condition, phase, and session of phase for each subject.

Results

To characterize respiratory phase-locked oscillations in the human brain, we analyzed iEEG data from depth electrodes inserted into PC, amygdala, and hippocampus in seven surgical epilepsy patients during natural breathing (five with PC coverage; all seven with amygdala and hippocampal coverage). As primary regions of interest, PC and amygdala receive direct afferent input the olfactory bulb (Carmichael et al., 1994; Root et al., 2014), and odor-evoked responses have been observed in human iEEG studies of amygdala (Hughes and Andy, 1979; Hudry et al., 2001; Jung et al., 2006). Hippocampus is not formally part of the olfactory network but receives projections from the olfactory system via the entorhinal cortex (Haberly and Price, 1978; Carmichael et al., 1994), and, in rodents, slow rhythmic activity in hippocampus can in some circumstances fluctuate in phase with nasal respiration (Macrides, 1975; Macrides et al., 1982; Kay, 2005; Viczko et al., 2014; Yanovsky et al., 2014; Kleinfeld et al., 2016; Nguyen Chi et al., 2016).

Slow oscillations in human piriform cortex are in synchrony with natural breathing

During data acquisition, patients breathed quietly through their noses, in the absence of odor stimulation, while respiration was monitored. Our initial analysis tested whether the ongoing rhythms of natural spontaneous breathing were in synchrony with slow fluctuations of neuronal activity. Qualitative inspection of these data suggested that the raw (unfiltered) LFP time series in PC was often in phase with breathing, with respiratory entrainment observed in each patient (Fig. 2*A*). To quantify these effects, a within-subject "event-related" analysis was performed in which the inspiratory peaks from the respiratory time series were used to define event-onset times (Fig. 3). First, the original LFP time series were filtered from 0 to 0.6 Hz, corresponding to the human respiratory range. The respiratory time series and the filtered LFP were then both organized into trials of 6 s duration, aligned to inspiratory peaks (from −2 to +4 s, with 0 being the inspiratory peak). Trials were averaged together, enabling us to compute the temporal correlation between the mean LFP signal and the mean respiratory signal on a patient-by-patient basis. This analysis revealed that in PC, the LFP was correlated with breathing in each patient, with *R* values ranging from 0.64 to 0.87 (Fig. 2*B*, red and blue traces).

The statistical significance of this effect was tested by plotting the correlation value (between LFP and respiratory signals) onto a distribution of randomly generated *R* values, in which the mean LFP signal was created from 6 s trials that were randomly chosen with respect to the inspiratory peak (Fig. 3). This process was iterated 1000 times (bootstrapping with resampling), yielding a statistically null distribution from which a *p* value could be calculated. As shown in Figure 2*C* (left column), the observed correlation value in PC was consistently outside of the upper bound of the 95% confidence interval of the randomly generated distribution for each and every patient, implying a significant time-series alignment between the LFP signal and breathing in this brain region (P1: $r = 0.64$, $p = 0.006$; P2: $r = 0.74$, $p = 0.008$; P3: $r = 0.87$, $p = 0.0001$; P4: $r = 0.72$, $p = 0.02$; P7: $r = 0.64$, $p = 0.002$), and in one patient in hippocampus (P1: $r = 0.77$, $p = 0.005$).

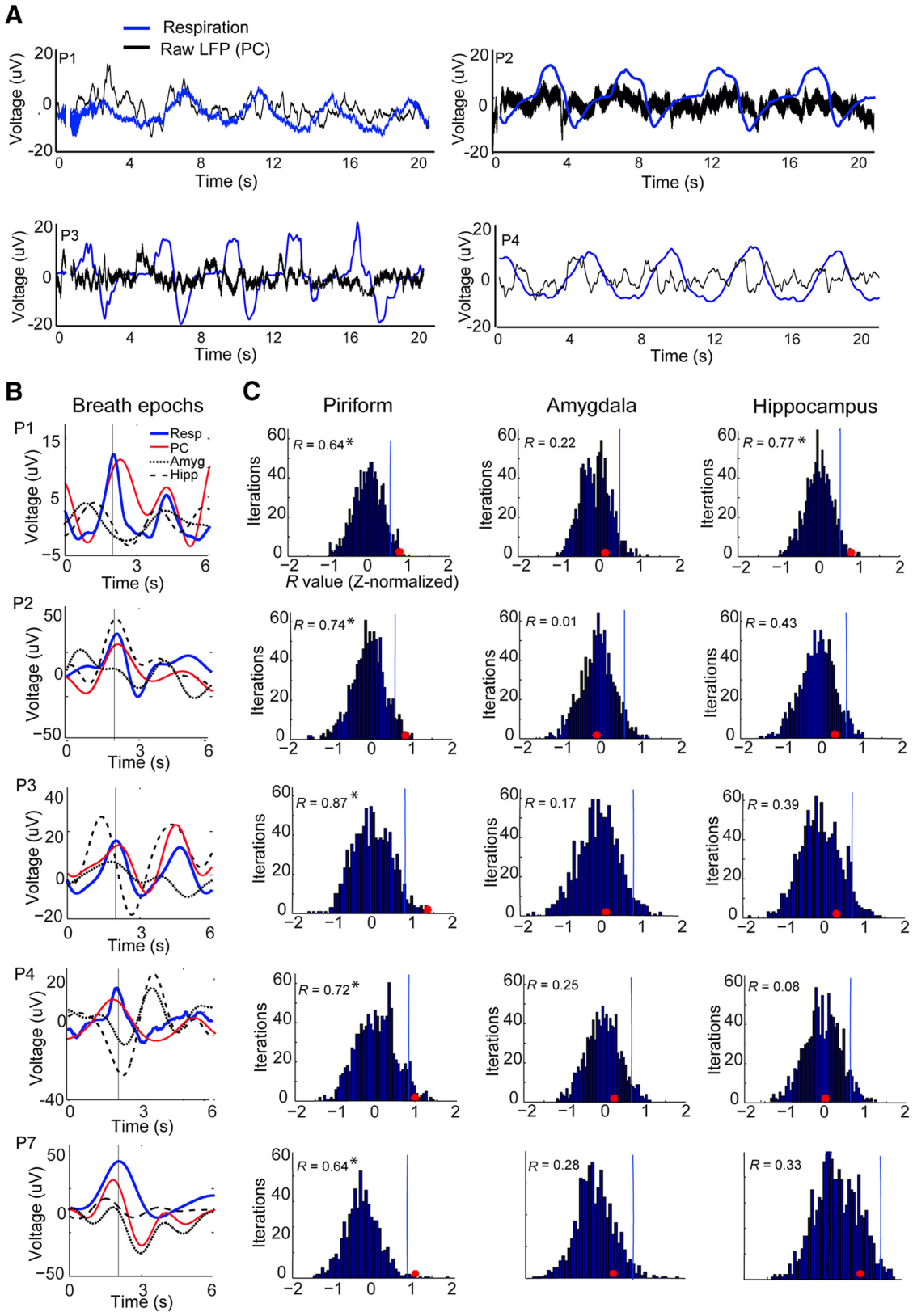

Figure 2. Slow oscillations in human PC are in phase with respiration. ***A***, Representative traces of the raw LFP time series from five patients with PC coverage show that slow fluctuations in PC (black) are in phase with inhalation (blue) across a series of breaths. Inspiration is in the upward direction in this and all panels. Patients are labeled, for example, as P1, P2, P3, etc., in chronological order of study enrollment. Note that the Nihon Kohden acquisition system allows recording oscillations as slow as 0.08 Hz, well below the respiratory range. ***B***, Patient-specific time-course plots depict the mean respiratory waveform (red) and the mean LFP signal in PC (black), amygdala (dotted line), and hippocampus (dashed line), filtered between 0 and 0.6 Hz, temporally aligned to the peak of inspiratory flow (at 2 s), and averaged over all trials. Across all patients, the LFP signal most consistently conforms to the respiratory rhythm in PC (each row represents data from one patient). ***C***, The correlation (*R* value) between the mean respiratory signal and the mean LFP signal is shown as a red dot for each patient in PC, amygdala, and hippocampus. These values are overlaid on histograms of *R* value null distributions (*z*-normalized) computed from 6 s LFP trials randomly aligned to the onset times of peak inspiratory flow. Correlations were statistically significant in all patients in PC. $^*p < 0.05$.

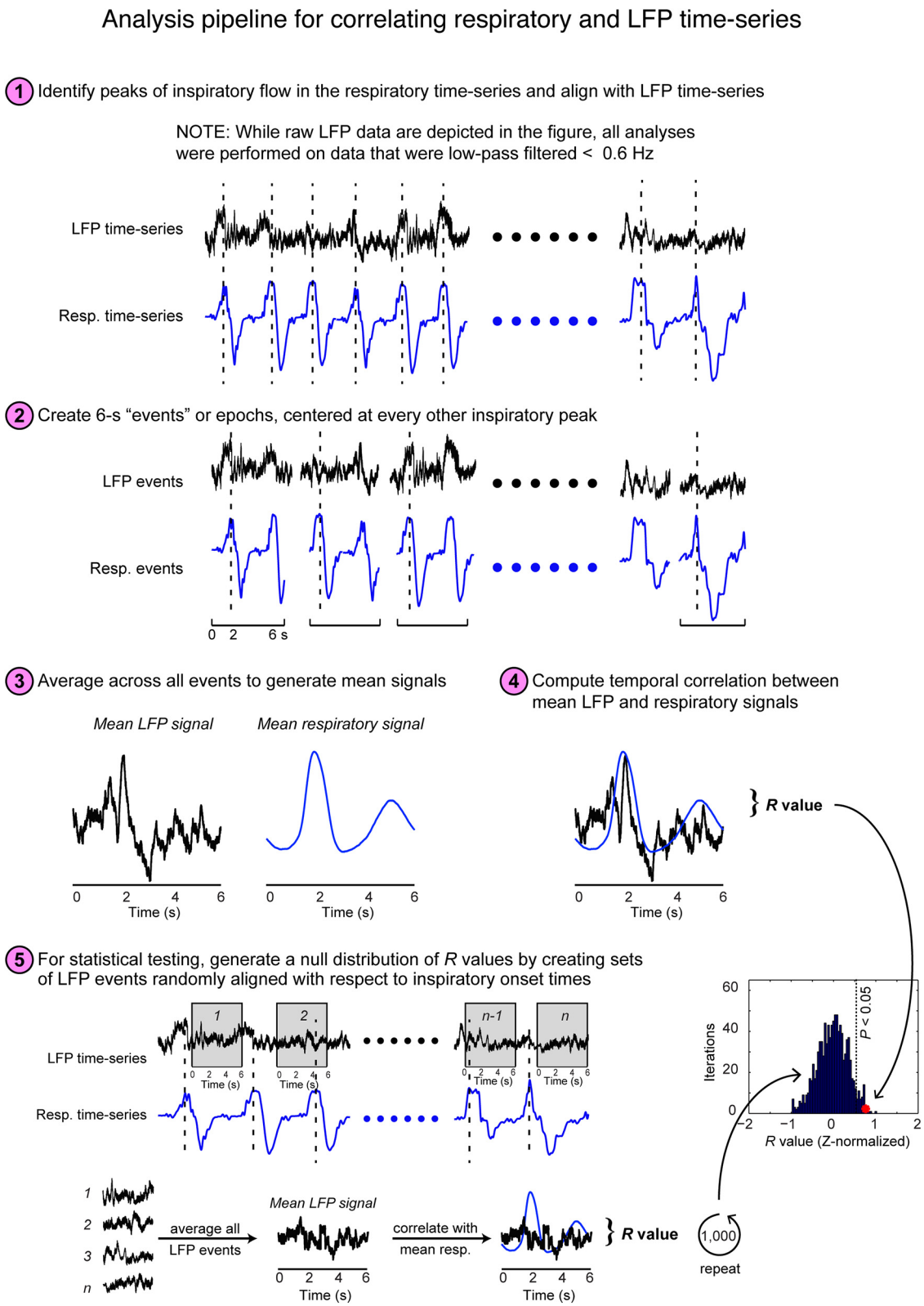

Figure 3. Analysis pipeline for correlating respiratory and LFP time series. (1) First, the respiratory data were synchronized with the LFP data, after being low-pass filtered at <0.6 Hz. (2) Data were then epoched into 6 s trials, aligned to inspiratory peak flow at time = 2 s, and extended from 2 to 4 s after inspiratory peaks. (Note, individual 6 s trials generally spanned more than one breath, and often included LFP data from the trial-aligned breath as well as partial data corresponding to the next breath). (3) Next, the inspiratory peak-aligned LFP trials were averaged to generate a mean 6 s waveform, and (4) the temporal correlation was computed between LFP and respiratory signals. (5) Finally, a null distribution was generated for statistical testing by creating LFP trials aligned randomly according to the respiratory data.

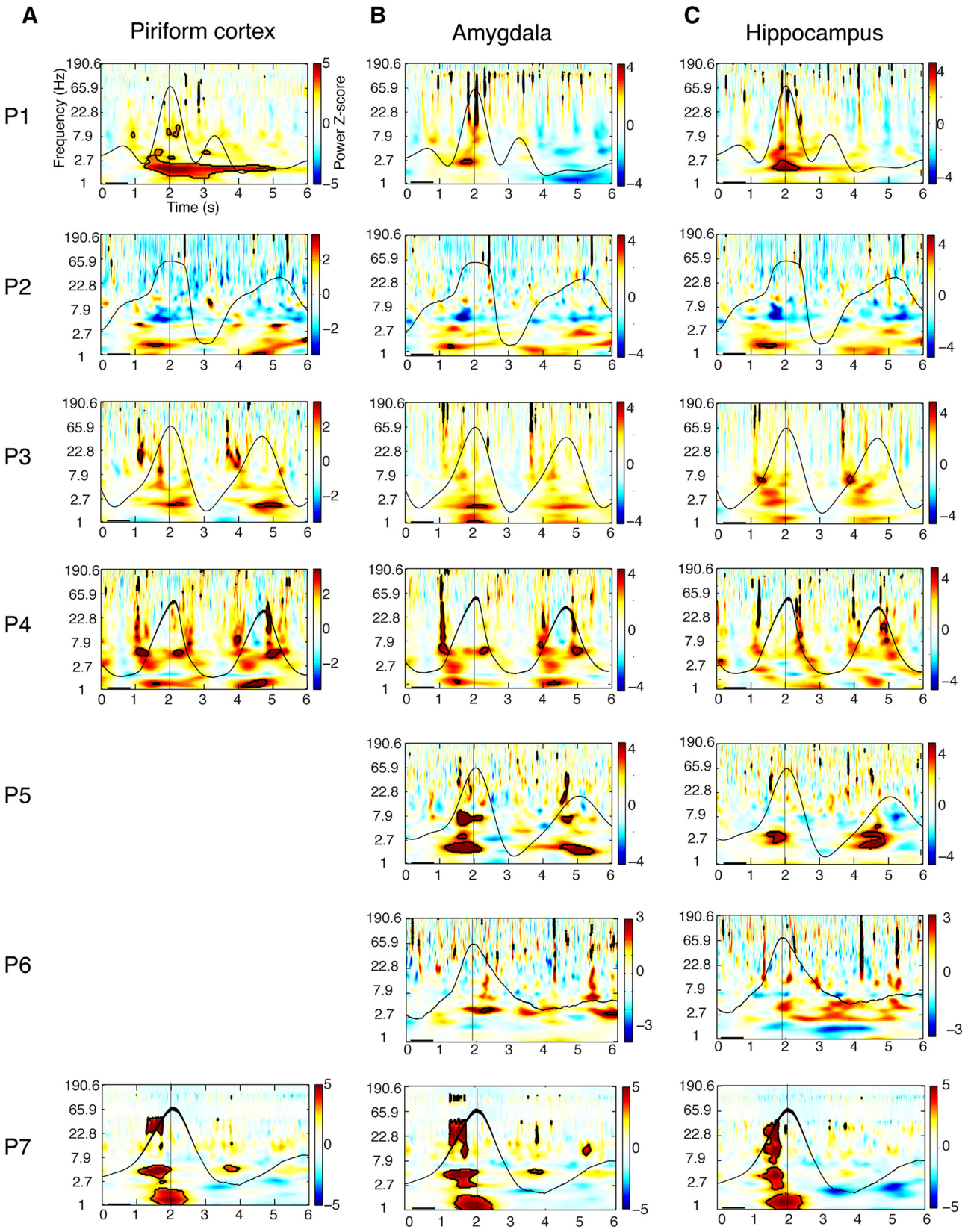

Figure 4. Respiration entrains higher-frequency oscillations in PC, amygdala, and hippocampus. ***A–C***, Time–frequency spectrograms for each patient were computed across trials and aligned to peak inspiratory flow at time = 2 s (vertical black lines). Each patient's averaged respiratory signal (black waveform) is overlaid on the corresponding spectrogram. The pseudocolor scale represents the mean spectral power (*z*-normalized) averaged over all breaths, on a patient-by-patient basis, relative to a preinhalation baseline period between 0.2 and 0.8 s (horizontal black bars). In PC (***A***) and amygdala (***B***), delta power significantly emerges during the inspiratory phase of breathing in each patient. Significant increases in delta power were also observed in hippocampus (***C***), although effects did not reach corrected significance in P3, P4, and P5. Time–frequency clusters, where spectral power survived statistical correction (FDR) for multiple comparisons (at $z > 3.2$), are outlined in black. Note, data from PC were not recorded in P5 and P6.

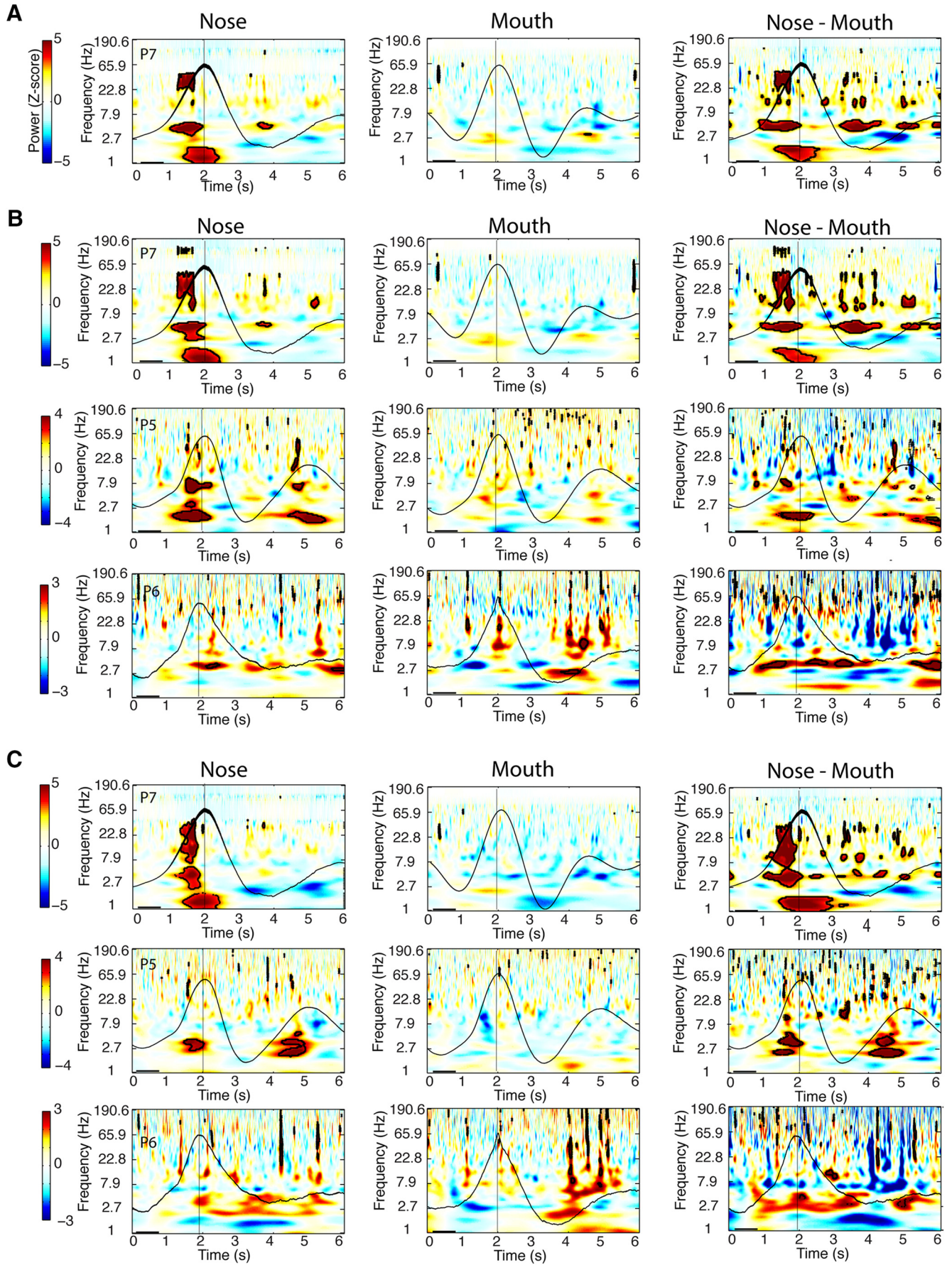
A
B
C
Nose
Mouth
Nose - Mouth
P7
P5
P6
Power (Z-score)
Frequency (Hz)
Time (s)

By comparison, respiratory-paced LFP fluctuations in other medial temporal lobe areas were not reliably aligned with breathing. In the amygdala (Fig. 2*B*,*C*, middle column), the correlation between neural and respiratory signals was low in all five patients (R value range, 0.01–0.25), none of which reached significance (p value range, 0.1–0.53). In the hippocampus (Fig. 2*B*,*C*, right column), correlation values were nonsignificant in four patients (R value range, 0.08–0.43; p value range, 0.13–0.44), with only one patient exhibiting significant respiratory entrainment (P1: $r = 0.77$; $p = 0.0001$). Together, these results highlight the specificity of these effects to the piriform olfactory area, and show that slow respiratory oscillations in PC are a characteristic electrophysiological signature of the human olfactory system, though at a much slower (~0.16–0.33 Hz) frequency of natural breathing than is observed in other mammalian model systems.

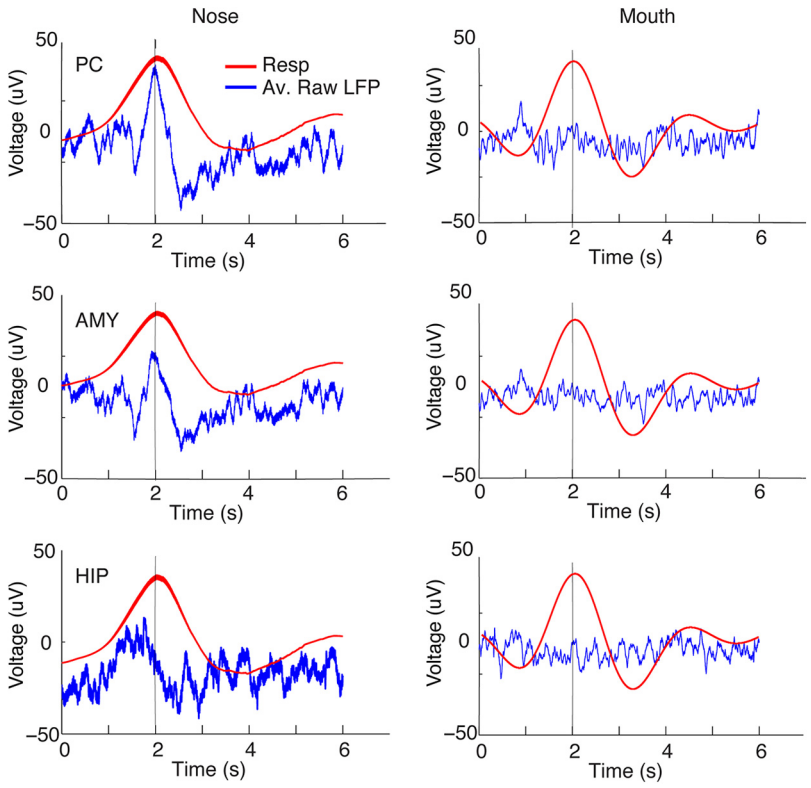

Figure 6. Comparison of slow respiratory oscillations in PC during nasal and oral breathing in P7. Top row, The correlation between the respiratory waveform and the raw (unfiltered) LFP time series in PC (averaged across 6 s breathing trials, aligned to peak inspiratory flow at time = 2 s) was robust during nasal breathing, but not during oral breathing. Middle and bottom rows, By comparison, in this same patient in amygdala (middle row) and hippocampus (bottom row), respiratory entrainment was not significant during either nasal or oral breathing.

Respiratory phase entrains higher-frequency limbic oscillations

Intracranial EEG recordings in animals and humans consistently show that higher-frequency oscillatory power is modulated by the phase of lower-frequency oscillations, enabling neuronal coordination across different time-scales (Fries, 2005; Canolty et al., 2006; Jensen and Colgin, 2007), and in some cases is even modulated by low-frequency rhythmic events, such as sounds (Lakatos et al., 2005) or quiet breathing (Moore et al., 2013; Ito et al., 2014; Rojas-Líbano et al., 2014). To test whether breathing phase systematically modulates oscillatory amplitudes at faster frequencies, we computed spectrograms averaged over trials, time locked to peak inhalation. Increases in oscillatory power were observed in PC in each and every patient (Fig. 4*A*), with spectral changes emerging during the inspiratory phase of breathing. Oscillatory power changes were consistent across patients, with statistically significant increases in the delta range (0.5–4 Hz) in every patient with PC coverage (P1, P2, P3, P4, and P7; z-scores > 3.2, FDR corrected for multiple corrections). All five patients with PC coverage also showed an inspiration-locked increase in the theta range (4–8 Hz), reaching statistical significance in all patients, though in smaller temporal clusters, and three patients (P3, P4, and P7) showed inspiration-locked increases in the beta range (13–30 Hz).

Respiratory entrainment was also observed in amygdala and hippocampus, with phase coupling arising near the onset of inspiration. In amygdala (Fig. 4*B*), inspiration-locked oscillatory power changes were similar to those in PC, with consistent increases in the delta range in all seven patients. Theta oscillations were less consistently locked to inspiration in this region, with three of seven patients showing theta power increases (P4, P5, and P7). In the hippocampus (Fig. 4*C*), all seven patients exhibited delta power increases following inspiration, though these effects survived FDR correction in only four patients (P1, P2, P5, and P7). Significant changes in hippocampal oscillatory power, again in phase with inspiration, were also found in the theta-frequency band (P1, P3, P4, P6, and P7) and in the beta-frequency band (P1, P4, P5, and P7). These findings indicate that respiratory phase-entrained oscillations in the human brain are not limited to olfactory-related regions, but extend to adjacent limbic networks in the medial temporal lobe, especially at low frequencies.

Human respiratory oscillations depend on nasal airflow

One mechanism by which respiratory phase and limbic cortical oscillations could become synchronized is that nasal airflow induces oscillatory activity in PC (Fontanini et al., 2003; Fontanini and Bower, 2005, 2006; Litaudon et al., 2008), which in turn propagates to amygdala and hippocampus via direct connections between these brain regions (Carmichael et al., 1994; Yanovsky et

←

Figure 5. Dependence of respiratory oscillations on nasal airflow. ***A–C***, Respiratory oscillations diminish when breathing is diverted from nose to mouth in PC (***A***), amygdala (***B***), and hippocampus (***C***). Time–frequency spectral plots are shown from one patient with PC coverage (P7), and three patients with amygdala and hippocampal coverage (P7, P5, and P6) who performed both nasal breathing (left panels) and oral breathing (middle panels) for 15 min each. (Spectrograms for the nasal breathing data are identical to those shown in Fig. 4.) The mean respiratory signals for nasal and oral respiration are plotted in black. The difference between nasal and oral spectrograms (nasal vs oral) is shown in the far right panels. Patients exhibited a consistent and significant decrement in respiratory oscillatory power from nasal to oral breathing for delta, theta, and beta frequency bands in PC, and for the delta frequency band in amygdala and hippocampus. Clusters outlined in black on the spectrograms survived FDR correction for statistical significance ($z > 3.2$).

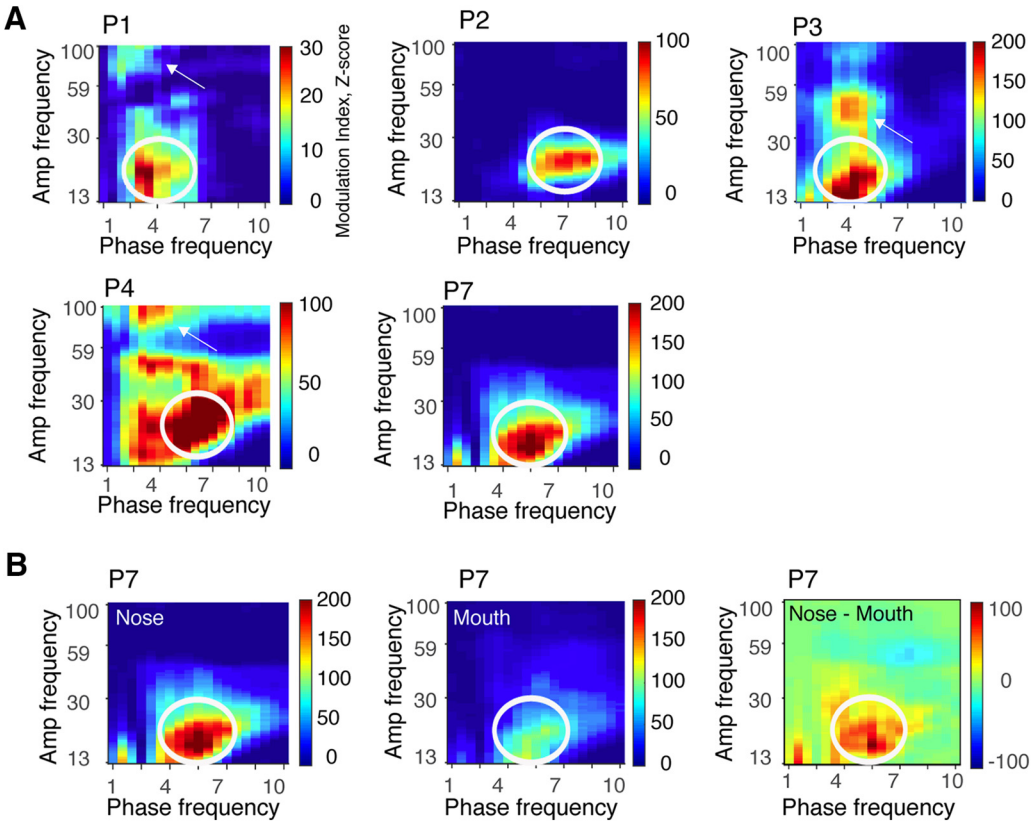

Figure 7. Consistent modulation of beta amplitude by theta phase in PC. ***A***, Comodulograms were computed individually in all five patients with piriform coverage, revealing cross-frequency coupling between theta phase and beta amplitude in each patient (white ovals). Each row represents one patient. Three of five patients also showed theta–gamma coupling (white arrows). Comodulograms were generated by computing the *z*-normalized MI for each phase-amplitude pair extending from 1 to 10 Hz in the phase dimension and from 13 to 200 Hz in the amplitude dimension. ***B***, In patient P7, the magnitude of cross-frequency coupling in PC was significantly diminished when breathing was directed through the mouth, as shown in the difference map between nasal and oral comodulograms (right). Note, the nasal comodulogram for P7 in this panel is identical to that shown for P7 in ***A***.

al., 2014). To test this hypothesis, we reasoned that if nasal airflow is critical for mediating limbic oscillations, then the diversion of airflow through the mouth should decrease respiratory entrainment in olfactory limbic areas. We examined iEEG data from three patients (P5, P6, and P7) who were asked to breathe naturally through either the nose or mouth in separate recording sessions. The order of nasal and oral breathing was counterbalanced across the patients. Electrode coverage for all three patients included amygdala and hippocampus (only P7 had PC coverage).

During oral (vs nasal) breathing, there was a distinct reduction of respiratory phase-locked oscillations in PC in the delta, theta, and beta ranges for each patient (Fig. 5*A*). The same breathing route-dependent decline in delta oscillatory activity was also evident in the amygdala and hippocampus for all three patients (Fig. 5*B*,*C*). These data indicate that the passage of air through the nose is critical for respiratory entrainment of delta and theta oscillations in PC, amygdala, and hippocampus. We found that nasal ($r = 0.64$, $p = 0.002$), but not oral ($r = 0.09$, $p > 0.05$) breathing was also critical for respiratory entrainment of the infraslow oscillations in PC (Fig. 6, top row). By comparison, respiratory entrainment was not significant during either nasal or oral breathing in amygdala (nasal breathing, $r = 0.28$; oral breathing, $r = 0.02$; p values >0.05) or hippocampus (nasal breathing, $r = 0.33$; oral breathing, $r = 0.42$; p values >0.05; Fig. 6, middle and bottom rows). While additional contributions from respiratory pacemakers in the brainstem cannot be discounted, our findings are compatible with the idea that respiratory-locked limbic oscillations originate from the cyclic movement of air through the nose, potentially propagating through PC en route to downstream targets in the medial temporal lobe.

Recent studies indicate that within-region modulation between the phase of a low-frequency LFP oscillation and the amplitude of a higher-frequency LFP oscillation (CFC) is enhanced in the human brain during high attentional demand, and has been linked to cognitive tasks not only in cortical brain regions (Schack et al., 2002; Schack and Weiss, 2005; Jensen and Colgin, 2007; Canolty and Knight, 2010; Voytek et al., 2010; Szczepanski et al., 2014), but also in deep limbic structures, such as the amygdala, hippocampus, and nucleus accumbens (Mormann et al., 2005; Tort et al., 2008; Cohen et al., 2009; Axmacher et al., 2010; Chaieb et al., 2015; Liu et al., 2015). CFC phenomena have also been observed during rest (Foster and Parvizi, 2012; Weaver et al., 2016) perhaps reflecting intrinsic oscillatory signatures among networks that are functionally connected (Foster and Parvizi, 2012). Whether the state of natural breathing through the nose is associated with phase-amplitude modulation across a particular frequency range in human olfactory areas has not been examined.

To this end, we estimated the MI value in PC, amygdala, and hippocampus for each combination of low-frequency phase (between 1 and 10 Hz) and higher-frequency amplitude (between 13 and 200 Hz; Tort et al., 2010) in each patient individually (see Materials and Methods). The resulting comodulograms revealed consistent clusters of CFC across patients in PC (Fig. 7), while the results were more dispersed and variable across subjects in amygdala and hippocampus (data not shown). Significant modulation of beta

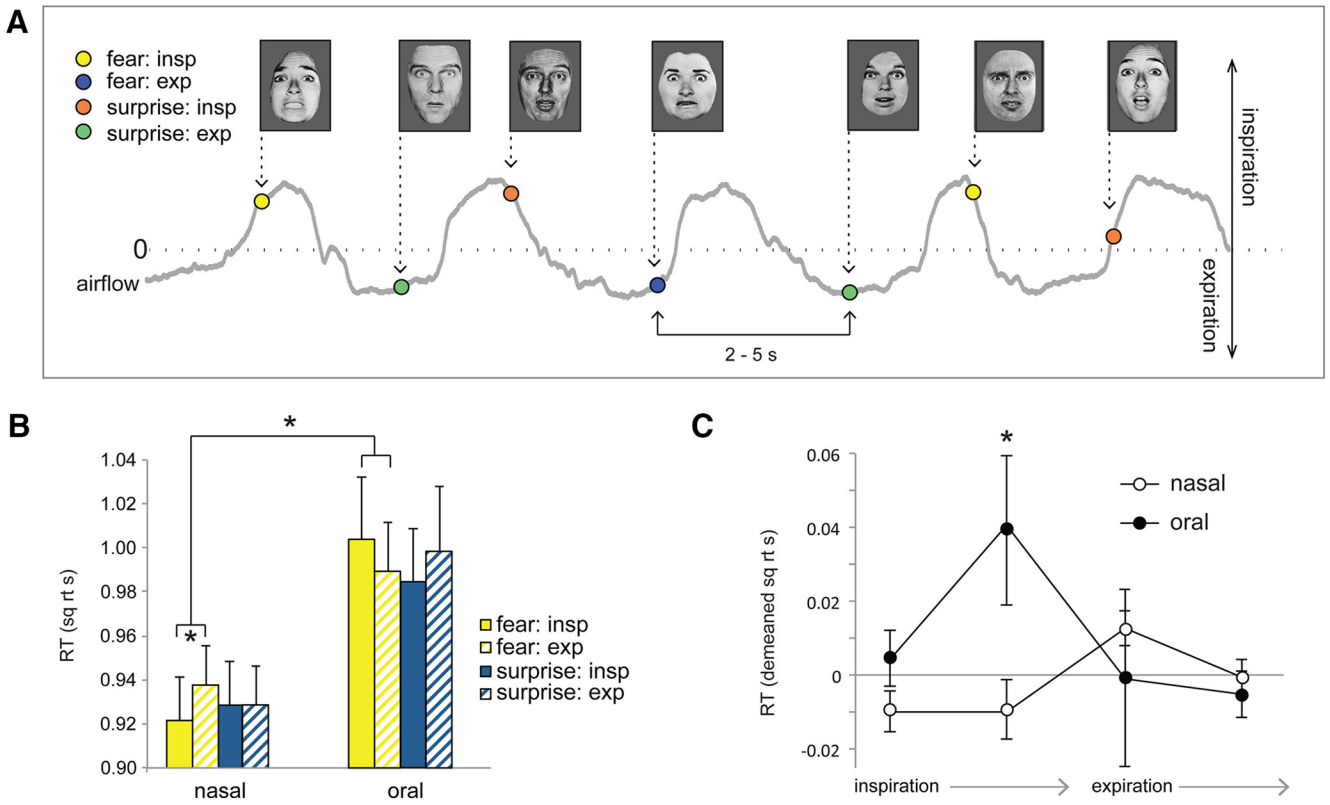

Figure 8. Respiratory phase modulates fear-related response times. ***A***, Emotion discrimination task. Subjects viewed faces expressing either fear or surprise, and indicated which emotion was perceived. Interstimulus interval, 2–5 s. Colored dots indicate where in the breathing cycle stimuli were encountered. ***B***, Fearful faces were detected more quickly during nasal inspiration vs expiration, but not during oral breathing. ***C***, Emotion RT data, binned across four phases of breathing, revealed a significant two-way interaction between breathing time bin (4 levels) and breathing route (nasal/oral) for fearful faces, with maximal RT differences during nasal fear trials occurring between the onset of inspiration and the onset of expiration. *$p < 0.05$ in all panels. Error bars represent the SEM.

power by theta phase was consistently present in PC in all five patients during nasal breathing (Fig. 7*A*, white ovals), as well as theta–gamma coupling in three of five patients (Fig. 7*A*, white arrows). In one patient with PC coverage (P7) who took part in the oral breathing task (Fig. 7*B*), there was a significant decrease in theta—beta coupling when breathing was diverted from nose to mouth, which is in line with the decrease in overall respiratory entrainment of LFP oscillations shown in Figure 6.

Respiratory phase and route modulate emotional response times in healthy subjects

Given that our data show markedly different patterns of neural activity in the amygdala and hippocampus during inhalation compared with exhalation, it follows that respiratory phase itself might have a fundamental impact on cognition. To test this hypothesis, we recruited independent groups of healthy subjects to participate in behavioral tasks typically associated with amygdala and hippocampal functions (see Materials and Methods). Critically, in these experiments, sensory stimuli (trials) were presented at random jittered intervals, enabling us to fully "tile" the breathing cycle and determine whether behavioral performance was enhanced when a stimulus arrived within a specific phase of respiration.

Based on the established role of the amygdala in the processing of fearful stimuli, we first examined whether the respiratory cycle modulates response times in an emotion discrimination task. Twenty-one subjects viewed rapid (100 ms) presentations of faces expressing either fear or surprise on separate trials, and made speeded responses to indicate which emotion was perceived (Fig. 8*A*). Fearful faces were identified more quickly when they had been encountered during inhalation compared with exhalation ($t_{(20)} = -2.64$, $p = 0.016$, paired t test, two-tailed), while no such effect was found for surprised faces ($t_{(20)} = -0.04$, $p = 0.97$, paired t test, two-tailed; Fig. 8*B*). In a separate group of subjects ($N = 17$) who breathed through their mouths instead of their noses, there was no effect on either fearful ($t_{(16)} = 1.21$, $p = 0.24$, paired t test, two-tailed) or surprised faces ($t_{(16)} = -1.08$, $p = 0.30$, paired t test, two-tailed), though there was a main effect of route (such that subjects were overall faster during nasal vs oral breathing; $F_{(1,36)} = 4.87$, $p = 0.03$). Critically, the specificity of this effect for the fear condition during nasal breathing was exemplified in the following two ways: the three-way interaction among airflow route (nasal/oral), emotion (fear/surprise), and respiratory phase (inspiration/expiration) was significant ($F_{(1,36)} = 4.77$, $p = 0.036$), and the two-way interaction between route (nasal/oral) and respiratory phase (inhale/exhale) for fearful faces was significant ($F_{(1,36)} = 5.83$, $p = 0.021$). The complementary two-way interaction of route and phase for surprised faces was not significant ($F_{(1,36)} = 1.004$, $p = 0.323$). Together, the above data establish the nasal origin of these effects.

By plotting time-series profiles of response times across four phase segments of the breathing cycle (Fig. 8*C*), we found that RTs significantly differed across phase time bins for the nasal route ($F_{(1,20)} = 4.98$, $p = 0.03$; repeated-measures ANOVA, main effect of phase) but not for the oral route ($F_{(1,16)} = 1.93$, $p = 0.18$). Importantly, the two-way interaction between route (two levels: nasal/oral) and phase time bin (four levels) was significant ($F_{(1,36)} = 5.48$, $p = 0.025$). In follow-up *post hoc* comparisons,

when the nasal group was examined separately, maximal RT differences across phases were observed between the beginning of inspiration and the beginning of expiration (Fig. 8*C*, point 1 vs point 3; $t_{(20)} = -3.0$, $p = 0.007$; two-tailed paired *t* test). Comparison between the nasal and oral groups shows that RTs were maximally different between the peak of inspiratory flow and the end of inspiration (point 2 in Fig. 8*C*; $t_{(36)} = -2.47$, $p = 0.016$; independent sample *t* test, two-tailed, fear nasal vs oral).

Although the above findings provide strong evidence for the selective effect of nasal breathing (vs oral breathing) on rapid emotional discrimination, it is possible that the oral breathing task could have introduced an attentional confound: subjects had to focus explicitly on keeping their mouth open, while simultaneously ensuring that air was not being directed through the nose. In this manner, if oral breathing had the effect of drawing subjects' attention away from the face stimuli, then this might have resulted in slower response times to those faces. Therefore, in a control behavioral experiment, we asked an independent group of subjects ($N = 24$) to perform the same emotion judgment task, while breathing through their nose but simultaneously keeping their mouth open. Because this maneuver poses the same distractions as the pure mouth-breathing task, we were able to assess whether greater attentional load (nasal breathing/mouth open) would abolish the RT differences between fearful and surprise faces.

Our results indicate that despite the imposed distraction, RTs remained significantly faster when faces were presented during inhalation compared with exhalation in the fear condition only ($t_{(23)} = -2.88$, $p = 0.009$; data not shown). Importantly, a comparison of fear RTs between the two experimental routes (nasal breathing vs nasal breathing/mouth open) revealed a significant main effect of breathing phase ($F_{(1,43)} = 14.81$, $p < 0.001$), with no significant interaction between route and phase ($F_{(1,43)} = 0.047$, $p = 0.83$). In parallel, when comparing nasal breathing/mouth open to oral breathing, we found no main effect of phase ($F_{(1,43)} = 0.53$, $p = 0.47$), whereas the interaction between route and phase was significant ($F_{(1,43)} = 6.62$, $p = 0.014$). These findings indicate that, despite the attentional demands of keeping the mouth open while breathing through the nose, the subject still responded more quickly to fearful faces during inhalation than during exhalation, with effects that significantly differed from oral breathing alone.

Analysis of the accuracy data from the emotion task indicates that subjects detected the fearful faces equally well during inspiration and expiration, without a significant difference between respiratory phases ($t_{(20)} = -1.71$, $p = 0.10$; data not shown). The same held true for surprised faces ($t_{(20)} = -0.70$, $p = 0.49$). When comparing nasal and oral routes, a three-way ANOVA among route, emotion, and phase yielded no significant main effects (route: $F_{(1,36)} = 0.90$, $p = 0.35$; emotion: $F_{(1,36)} = 0.25$, $p = 0.62$; phase: $F_{(1,36)} = 1.16$, $p = 0.29$), two-way interactions (route by emotion: $F_{(1,36)} = 0.48$, $p = 0.49$; route by phase: $F_{(1,36)} = 0.48$, $p = 0.492$; emotion by phase: $F_{(1,36)} = 1.87$, $p = 0.18$), or three-way interaction ($F_{(1,36)} = 0.78$, $p = 0.38$).

Respiratory phase modulates recognition memory accuracy in healthy subjects

Finally, given the role of the hippocampus in memory function, independent sets of subjects took part in an object recognition memory task. Subjects first viewed pictures of visual objects presented at random time intervals to fully tile the respiratory cycle (Fig. 9*A*). After a 20 min break, subjects were presented with the old pictures plus an equal number of new pictures, again at random time intervals. Trials were then sorted according to the respiratory phase in which the pictures had initially been presented, and also according to the respiratory phase of the picture during retrieval. In subjects who breathed through the nose ($N = 11$), breathing phase exerted an overall significant main effect on recognition accuracy ($F_{(1,10)} = 6.18$, $p = 0.03$; two-way ANOVA), whereby accuracy was enhanced for the pictures that had been retrieved during inspiration versus expiration ($t_{(10)} = 2.85$, $p = 0.017$, paired *t* test, two-tailed; Fig. 9*B*).

Such phase-specific effects on recognition accuracy were not observed in subjects who breathed orally ($N = 11$; $t_{(10)} = -1.07$, $p = 0.31$), and there was no main effect of route (nasal vs oral) on overall accuracy ($F_{(1,20)} = 1.15$, $p = 0.29$). Critically, in the two-way interactions of phase-by-route, inhalation (vs exhalation) had a significantly stronger impact on memory performance during nasal versus oral breathing, both for encoding ($F_{(1,20)} = 4.51$, $p = 0.046$) and retrieval ($F_{(1,20)} = 7.06$, $p = 0.015$; Fig. 9*B*). In other words, retrieval accuracy was higher for those picture items that had been encoded during the inspiratory phase of breathing, and was also higher for picture items retrieved during inspiration, for the nasal route only.

The above data indicate that, during the encoding session, the (nasal) respiratory phase had a significant effect on subsequent memory in the retrieval session, with greater accuracy for pictures encoded during inspiration (vs expiration) and for pictures retrieved during inspiration (vs expiration). However, this analysis was averaged across all trials, and was therefore unable to determine whether memory recognition was selectively enhanced when the same pictures were encountered in same (or different) respiratory phases across encoding and retrieval sessions. For example, one possibility would be that recognition memory for pictures appearing in the inspiratory phase during retrieval would be selectively enhanced for those same pictures that had appeared in the inspiratory phase during encoding.

To explore this question, we conducted a follow-up analysis in which all "hit" trials (pictures successfully recognized during retrieval) were sorted into the following four categories: (1) pictures encoded in inspiration that were retrieved in inspiration; (2) pictures encoded in expiration that were retrieved in inspiration; (3) pictures encoded in inspiration that were retrieved in expiration; and (4) pictures encoded in expiration that were retrieved in expiration. This arrangement conformed to a 2×2 factorial design, with factors of encoding session phase (inspiration/expiration) and retrieval session phase (inspiration/expiration). A two-way repeated-measures ANOVA revealed a main effect of retrieval phase ($F_{(1,10)} = 7.00$, $p = 0.025$), but no main effect of encoding phase ($F_{(1,10)} = 0.95$, $p = 0.35$), and no interaction between encoding and retrieval phases ($F_{(1,10)} = 0.17$, $p = 0.69$). These data indicate that the inspiratory (vs expiratory) phase of breathing during memory retrieval had a greater impact on picture recognition, although memory performance did not depend on whether those same pictures had appeared in the same or a different respiratory phase at the time of encoding (Fig. 9*C*).

We also asked an independent group of subjects ($N = 11$) to take part in the same memory paradigm while performing the attention control task (nasal breathing while holding the mouth open). In comparing the nasal breathing group to the control (nasal breathing/mouth open) group, there remained a main effect of phase during retrieval ($F_{(1,20)} = 5.48$, $p = 0.030$), without a main effect of route ($F_{(1,20)} = 1.96$, $p = 0.18$), and without an interaction of phase by route ($F_{(1,20)} = 4.0$, $p = 0.059$), suggesting that attentional demands did not have a marked effect on memory performance. Analysis of the RT data from the memory task indicates that breathing phase had no main effect on response

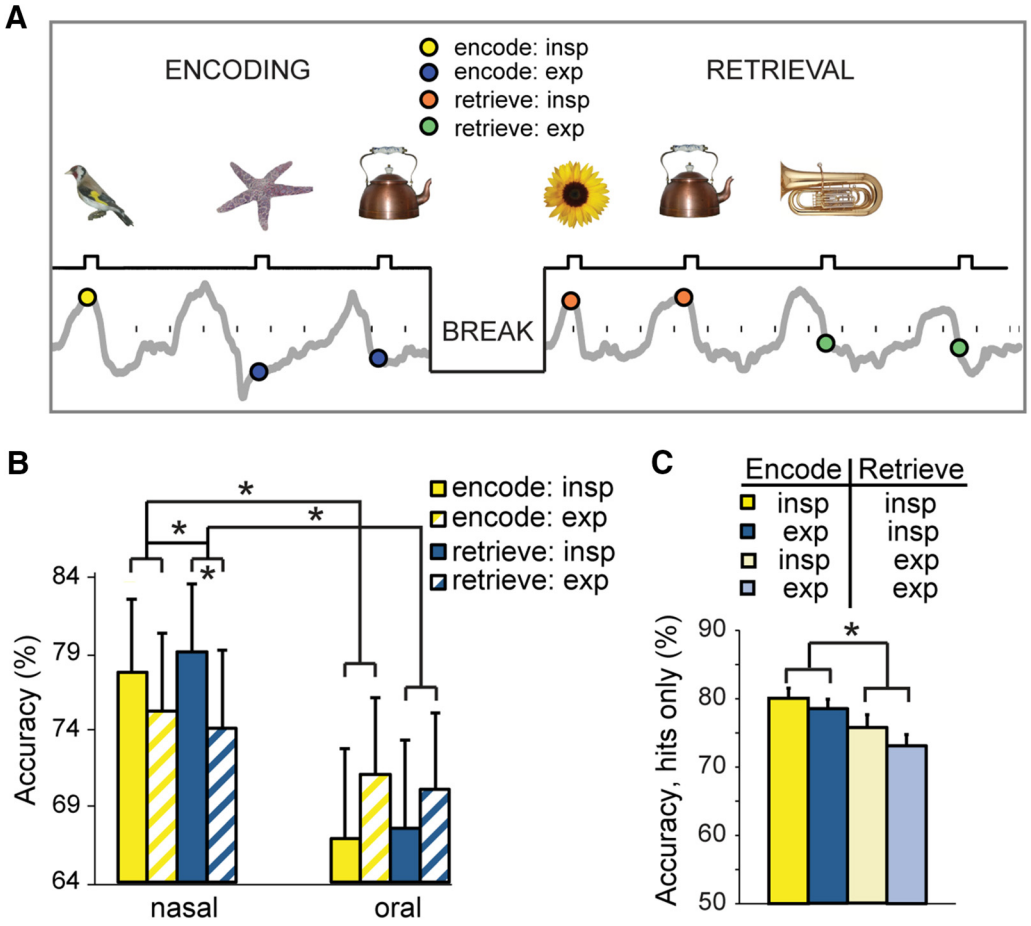

Figure 9. Respiratory phase modulates episodic memory performance. ***A***, In a recognition memory task, subjects viewed a series of different visual objects that occurred at different times within the breathing cycle. Interstimulus interval, 3–6 s. After a 20 min break, subjects were presented with the old pictures from the encoding session plus an equal number of new pictures. ***B***, Memory performance was more accurate during inspiration than during expiration, with effects more pronounced for nasal than oral breathing, both for encoding and retrieval. ***C***, An analysis of all "hit" trials revealed that recognition memory was significantly enhanced for pictures that had appeared during the inspiratory (vs expiratory) phase of retrieval, but it made no difference whether those same pictures had been encountered in the same phase during encoding. $*p < 0.05$ in all panels.

times during memory retrieval when subjects breathed through their noses ($t_{(10)} = 0.48$, $p = 0.64$), through their mouths ($t_{(10)} = -0.27$, $p = 0.79$), or through their noses while keeping their mouths open ($t_{(10)} = 0.12$, $p = 0.90$).

Amygdala inspiratory power in one patient predicts performance on an emotion judgment task

To identify a direct relationship between respiratory oscillatory entrainment and cognitive modulation, we obtained intracranial EEG data from one additional patient (P8) with amygdala coverage who participated in the emotion discrimination task (Fig. 10), on each trial indicating whether the face was expressing fear or surprise. During this task, the patient identified fearful faces more quickly during inspiration than expiration. Although there was no significant difference in response times for fear versus surprise trials, or for inhalation versus exhalation trials (all p values >0.14), the interaction between respiratory phase and emotion was significant, and in the predicted direction ($F_{(1,128)} = 3.446$, $p = 0.03$, one-tailed; Fig. 10*A*). In an initial analysis, we simply tested whether respiratory phase had a modulatory effect on LFP oscillatory activity in the amygdala. The time–frequency spectrogram, based on an average of all 6 s trials (time locked to peak inspiratory flow, as in Fig. 4), revealed oscillatory power increases in the delta-, theta-, and beta-frequency bands (Fig. 10*B*), in line with the demonstration of low-frequency respiratory entrainment observed in the other seven patients.

To look for a direct relationship between oscillatory power during inhalation and response times, we conducted a trial-by-trial analysis of the amygdala LFP data (limited to the 24 trials in which fearful faces appeared during inhalation). On trials where the patient identified the face more rapidly, we found that the inspiratory delta power was generally higher (Fig. 10*C*). To quantify this effect, trialwise RTs were regressed onto mean inspiratory power (within the delta band), revealing a significant correlation between these two measures (Fig. 10*D*, top left; $r = -0.4$, $p = 0.05$). By comparison, such relationships were not observed when examining mean expiratory power during fear trials ($r = 0.15$, $p = 0.33$), nor during surprise trials for either mean inspiratory ($r = 0.13$, $p = 0.47$) or mean expiratory ($r = 0.01$, $p = 0.95$) power (Fig. 10). Although preliminary, the demonstration of an inverse relationship between the magnitude of respiratory oscillatory entrainment in the amygdala and reaction times on the emotion task provides an important bridge between the electrophysiological and behavioral datasets, and brings support to the idea that respiratory limbic oscillations can shape cognitive performance.

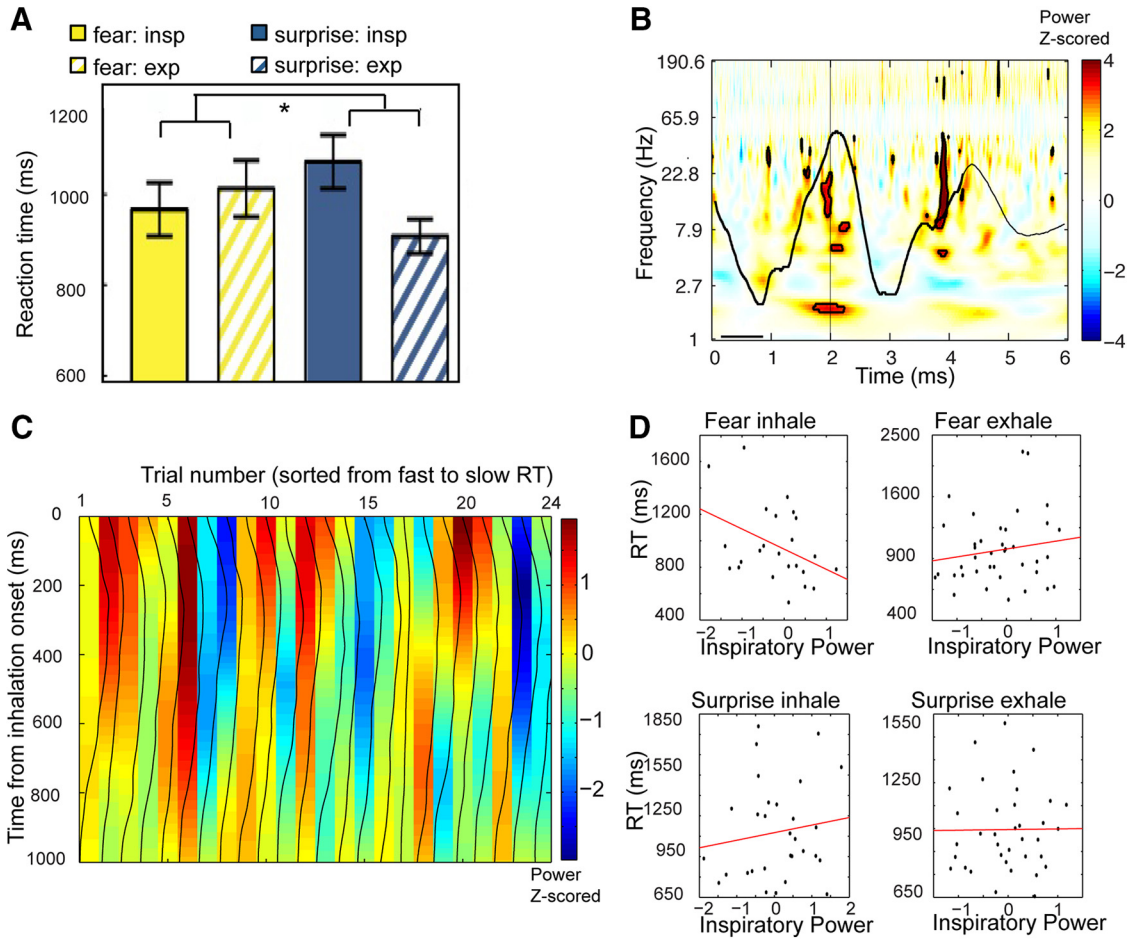

Figure 10. Strength of respiratory modulation in the amygdala predicts emotional response times. ***A***, One patient (P8) with intracranial coverage of the amygdala participated in the emotion discrimination task (as in Fig. 8). Analysis of RTs revealed a significant interaction between emotion (fear vs surprise) and respiratory phase (inhale vs exhale). ***B***, A time–frequency spectrogram computed across all breaths highlights respiratory entrainment of oscillatory activity in the amygdala, as observed in the patients who took part in the passive breathing task. Significant spectral clusters (FDR-corrected) are outlined in black, and include delta-, theta-, and beta-frequency bands. Black line, Respiratory waveform; black horizontal bar, preinspiratory baseline period used for *z*-normalization. ***C***, In a trial-by-trial analysis of inspiratory delta power, the 24 trials in which fearful faces appeared during the inspiratory phase of breathing were sorted by increasing RT, and suggest that fear–inhalation trials with higher oscillatory entrainment in amygdala (orange-to-red colors) were generally associated with faster behavioral responses, compared with trials associated with slower behavioral responses (green-to-blue colors). The respiratory signal for each trial is overlaid (vertically from top to bottom) in black. ***D***, Trial-by-trial scatterplots of amygdala delta power vs emotion judgment RTs demonstrated a significant negative correlation for fear–inhalation trials only, whereby trials with greater inspiratory power were associated with lower (faster) RTs. Trialwise measures of amygdala delta power were averaged across the entire time-window of inhalation or exhalation separately for fear and surprise conditions.

Discussion

Beginning with the groundbreaking work of Lord Adrian almost 75 years ago (Adrian, 1942, 1950), the presence of respiratory oscillations has become a defining electrophysiological signature of the olfactory system, yet no published study has demonstrated this phenomenon in humans. By using iEEG techniques to measure oscillatory activity directly from the human brain, we show that electrical fluctuations in human PC are in phase with the natural cycle of breathing. This respiratory synchrony extends across both temporal and spatial scales, with higher-frequency oscillatory entrainment not only in PC, but also in amygdala and hippocampus. Our findings thus establish that the phasic respiratory organization of electrical activity in the olfactory system of small mammals is equally applicable to the human olfactory system, despite the fact that humans breathe at a dramatically slower rate.

Natural breathing paces slow respiratory oscillations in human piriform cortex

Intriguingly, the slow rate of human respiration approaches the range of "infraslow" oscillations that were first observed in animals >50 years ago (Aladjalova, 1957). The mechanism by which the brain generates infraslow electrical fluctuations likely involves multiple intracerebral structures, with animal studies indicating self-sustaining infraslow fluctuations in cortical slices (Sanchez-Vives et al., 2000; Timofeev et al., 2000), as well as evidence for non-neuronal contributions from glial cells (Dietzel et al., 1989; Amzica and Steriade, 2000; Heinemann et al., 2000; Laming et al., 2000) and the blood–brain barrier (Vanhatalo et al., 2003; Voipio et al., 2003). Speculatively, the large amplitude and long duration of infraslow oscillations suggests a likely contribution from subcortical structures as well (Usher et al., 1999). In humans, infraslow oscillations have been linked to resting-state oscillatory networks (Mantini et al., 2007; Picchioni et al., 2011; Hiltunen et al., 2014), and studies have also found coherence between fMRI BOLD signal and respiration in olfactory cortex (Sobel et al., 1998; Mainland and Sobel, 2006). The data presented here suggest the possibility of an additional unique source of infraslow activity: air plumes that periodically enter the nose at the rate of quiet breathing may elicit slow and rhythmic neuronal oscillations that propagate throughout limbic brain networks.

The inspiratory phase of breathing entrains higher-frequency oscillations in the human medial temporal lobe including piriform cortex

We also found that respiratory entrainment of higher-frequency limbic oscillations was consistent across patients. The inspiratory phase of nasal breathing was associated with increased power in the delta frequency range in each of five patients in PC, and seven patients in amygdala and hippocampus (Fig. 4), with effects surviving statistical correction for multiple comparisons. The relevance of nasal airflow for respiratory cortical entrainment was established in separate experiments where three patients breathed through either the nose or the mouth. Diversion from nasal to oral breathing led to a disorganization of limbic oscillatory synchrony in all three brain regions. Of note, the emergence of cross-frequency coupling between theta phase and beta amplitude in PC also dissipated when the breathing route was switched from nose to mouth (Fig. 7). Mechanistically, such findings imply that variations in low-frequency (delta) power, itself under the infraslow pace of nasal respiration, serve as a carrier rhythm on which oscillations at faster frequencies are embedded, or nested, within the limbic system (Lakatos et al., 2005). More generally, the demonstration that respiratory phase-locked oscillations—and their coupling to higher-frequency rhythms—are driven by nasal inhalation suggests that this breathing route serves as a common "clock" to organize spatiotemporal excitability broadly throughout the brain (Kay, 2005; Fontanini and Bower, 2006; Moore et al., 2013; Ito et al., 2014; Yanovsky et al., 2014).

Cross-frequency coupling is thought to play an important role in coordinating neural activity across different spatial and temporal scales, potentially underlying neural information processing and cognition (Bragin et al., 1995; Lisman and Idiart, 1995; Canolty et al., 2006; Tort et al., 2009; Axmacher et al., 2010; Canolty and Knight, 2010; Palva et al., 2010; Lisman and Jensen, 2013; Szczepanski et al., 2014; Aru et al., 2015). Maximal modulation has most commonly been reported between theta phase and gamma amplitude in cortical areas. Interestingly, we found a different frequency profile for CFC in human olfactory cortex, namely, theta phase modulating beta (rather than gamma) amplitude. Enhanced theta–beta coupling in olfactory cortex was consistently present in all five subjects with PC coverage, lending strength to our findings, and dovetailing nicely with data from rodents suggesting that beta oscillations dominate the LFP during odor sampling (Neville and Haberly, 2003; Lowry and Kay, 2007; Martin et al., 2007; Poo and Isaacson, 2009; Kay and Beshel, 2010). Such forms of neurophysiological convergence across different species suggest that human intracranial EEG approaches may play an important role in helping to inform and constrain mechanistic principles of olfactory system function in animal models where causal hypotheses can be more easily addressed.

The respiratory phase of nasal breathing modulates limbic-based behaviors

A key implication of our data is that the nasal route of respiration offers an entry point to limbic brain areas for modulating cognitive function. Indeed, behavioral data across three experiments and 62 participants demonstrated that respiratory phase and route have a significant influence on emotion discrimination and recognition memory. Independent groups of healthy subjects were better able to recognize fearful expressions, and were better able to retrieve visual object memories, when target stimuli were encountered during nasal inspiration than during expiration. We also found that the route of breathing was critical to these effects, such that cognitive performance significantly declined during oral breathing. Importantly, the effects of nasal breathing on cognition were sustained even when subjects were asked to hold their mouth open, helping to control for attentional confounds that might have arisen during the oral breathing experiment. Together, these findings support the idea that passive inhalation of air through the nose can selectively enhance reaction times to fearful stimuli and the accuracy of visual object recognition.

Combined behavioral and electrophysiological data from one patient show that respiratory entrainment of LFP activity in the amygdala is predictive of performance on an emotion discrimination task. In linking trial-by-trial changes in respiratory oscillations to behavior, these results bring insights into the potential mechanisms by which breathing can influence human cognitive processing. That rhythmic breathing paces electrical activity in the human brain to modulate behavior raises the intriguing possibility that other physiological and autonomic rhythms, and even periodic sampling in other sensory domains (Kepecs et al., 2006; Moore et al., 2013; Ito et al., 2014), might also shape neuronal oscillations to optimize human perception, emotion, and cognition. We would note that, while the effect sizes of our behavioral results are relatively modest (e.g., a 28 ms difference between fear inhalation and fear exhalation for the nasal route; a 60 ms difference between fear inhalation/exhalation for the nasal vs oral route), the magnitude of the changes is on par with those found in many other cognitive studies examining the effects of facial emotion on perceptual discrimination, with differences typically in the range of 20–100 ms (Doty et al., 2014; Li et al., 2014; Ye et al., 2014).

While our iEEG data provide direct evidence for respiratory phase-specific entrainment in the human brain, the use of iEEG methods has inherent shortcomings. Limited availability of epilepsy research patients for these studies means that sample sizes tend to be low. Because medication regimen, postimplantation hospital course, and regional locations of the electrodes are just a few of the many factors that may differ across patients, data variability across patients can be high. To minimize these issues, and to prevent outlier bias effects, we conducted and presented all analyses at the level of individual patients, and highlighted common electrophysiological profiles across patients. In the context of our study, attentional fluctuations, breathing differences, and temporal jitter (associated with event-related spectral analyses) are additional potential sources of variability that might have emerged both within and between patients. Nevertheless, the fact that our effects were generally consistent across patients, and survived statistical correction for multiple comparisons, suggests that this variance did not have a major detrimental impact and would only have reduced the strength of our findings.

In demonstrating respiratory modulation of cognition, our data provide a novel counterpoint to earlier studies reporting cognitive (behavioral) modulation of respiration. Animals routinely increase their respiratory rate during exploratory behavior (Welker, 1964; Kay and Freeman, 1998; Verhagen et al., 2007; Evans et al., 2009; Vlemincx et al., 2011; Huijbers et al., 2014), and humans alter their respiratory patterns in response to emotional stimuli (Boiten, 1998) and cognitive effort (Evans et al., 2009; Vlemincx et al., 2011; Huijbers et al., 2014). For example, the human respiratory cycle phase locks to stimulus presentations during memory encoding (Huijbers et al., 2014), and respiratory variability is reduced during mental load and attentional tasks (Vlemincx et al., 2011). Such studies suggest that respiratory patterns are impacted by cog-

nition, but do not address the possibility that the respiratory rhythm directly impacts neural activity in the brain in a functionally relevant manner. Our findings imply that, rather than being a passive target of heightened arousal or vigilance, the phase of natural breathing is actively used to promote oscillatory synchrony and to optimize information processing in brain areas mediating goal-directed behaviors.

References

Adrian ED (1942) Olfactory reactions in the brain of the hedgehog. J Physiol 100:459–473. CrossRef Medline

Adrian ED (1950) Sensory discrimination—with some recent evidence from the olfactory organ. Br Med Bull 6:330–333. Medline

Aladjalova NA (1957) Infra-slow rhythmic oscillations of the steady potential of the cerebral cortex. Nature 179:957–959. CrossRef Medline

Amzica F, Steriade M (2000) Neuronal and glial membrane potentials during sleep and paroxysmal oscillations in the neocortex. J Neurosci 20:6648–6665. Medline

Aru J, Aru J, Priesemann V, Wibral M, Lana L, Pipa G, Singer W, Vicente R (2015) Untangling cross-frequency coupling in neuroscience. Curr Opin Neurobiol 31:51–61. CrossRef Medline

Axmacher N, Henseler MM, Jensen O, Weinreich I, Elger CE, Fell J (2010) Cross-frequency coupling supports multi-item working memory in the human hippocampus. Proc Natl Acad Sci U S A 107:3228–3233. CrossRef Medline

Benjamini Y, Hochberg Y (1995) Controlling the false discovery rate-a practical and powerful approach to multiple testing. J R Stat Soc Series B Stat Methodol 57:289–300.

Boiten FA (1998) The effects of emotional behaviour on components of the respiratory cycle. Biol Psychol 49:29–51. CrossRef Medline

Bragin A, Jandó G, Nádasdy Z, Hetke J, Wise K, Buzsáki G (1995) Gamma (40–100 hz) oscillation in the hippocampus of the behaving rat. J Neurosci 15:47–60. Medline

Brainard DH (1997) The psychophysics toolbox. Spat Vis 10:433–436. CrossRef Medline

Bruns A (2004) Fourier-, Hilbert- and wavelet-based signal analysis: are they really different approaches? J Neurosci Methods 137:321–332. CrossRef Medline

Canolty RT, Knight RT (2010) The functional role of cross-frequency coupling. Trends Cogn Sci 14:506–515. CrossRef Medline

Canolty RT, Edwards E, Dalal SS, Soltani M, Nagarajan SS, Kirsch HE, Berger MS, Barbaro NM, Knight RT (2006) High gamma power is phase-locked to theta oscillations in human neocortex. Science 313:1626–1628. CrossRef Medline

Canolty RT, Soltani M, Dalal SS, Edwards E, Dronkers NF, Nagarajan SS, Kirsch HE, Barbaro NM, Knight RT (2007) Spatiotemporal dynamics of word processing in the human brain. Front Neurosci 1:185–196. CrossRef Medline

Cao Y, Roy S, Sachdev RN, Heck DH (2012) Dynamic correlation between whisking and breathing rhythms in mice. J Neurosci 32:1653–1659. CrossRef Medline

Carmichael ST, Clugnet MC, Price JL (1994) Central olfactory connections in the macaque monkey. J Comp Neurol 346:403–434. CrossRef Medline

Chaieb L, Leszczynski M, Axmacher N, Höhne M, Elger CE, Fell J (2015) Theta-gamma phase-phase coupling during working memory maintenance in the human hippocampus. Cogn Neurosci 6:149–157. CrossRef Medline

Cohen MX (2014) Analyzing neural time series data: theory and practice. Cambridge, MA: MIT.

Cohen MX, Axmacher N, Lenartz D, Elger CE, Sturm V, Schlaepfer TE (2009) Good vibrations: cross-frequency coupling in the human nucleus accumbens during reward processing. J Cogn Neurosci 21:875–889. CrossRef Medline

Delorme A, Makeig S (2004) EEGLAB: an open source toolbox for analysis of single-trial EEG dynamics including independent component analysis. J Neurosci Methods 134:9–21. CrossRef Medline

Dietzel I, Heinemann U, Lux HD (1989) Relations between slow extracellular potential changes, glial potassium buffering, and electrolyte and cellular volume changes during neuronal hyperactivity in cat brain. Glia 2:25–44. CrossRef Medline

Doty TJ, Japee S, Ingvar M, Ungerleider LG (2014) Intersubject variability in fearful face processing: the link between behavior and neural activation. Cogn Affect Behav Neurosci 14:1438–1453. CrossRef Medline

Eichenbaum H, Yonelinas AP, Ranganath C (2007) The medial temporal lobe and recognition memory. Annu Rev Neurosci 30:123–152. CrossRef Medline

Ekman P, Friesan WV (1975) Unmasking the face: a guide to recognizing emotions from facial clues. Englewood Cliffs, NJ: Prentice-Hall.

Evans KC, Dougherty DD, Schmid AM, Scannell E, McCallister A, Benson H, Dusek JA, Lazar SW (2009) Modulation of spontaneous breathing via limbic/paralimbic-bulbar circuitry: an event-related FMRI study. Neuroimage 47:961–971. CrossRef Medline

Fontanini A, Bower JM (2005) Variable coupling between olfactory system activity and respiration in ketamine/xylazine anesthetized rats. J Neurophysiol 93:3573–3581. CrossRef Medline

Fontanini A, Bower JM (2006) Slow-waves in the olfactory system: an olfactory perspective on cortical rhythms. Trends Neurosci 29:429–437. CrossRef Medline

Fontanini A, Spano P, Bower JM (2003) Ketamine-xylazine-induced slow (<1.5 Hz) oscillations in the rat piriform (olfactory) cortex are functionally correlated with respiration. J Neurosci 23:7993–8001. Medline

Foster BL, Parvizi J (2012) Resting oscillations and cross-frequency coupling in the human posteromedial cortex. Neuroimage 60:384–391. CrossRef Medline

Frederick DE, Brown A, Brim E, Mehta N, Vujovic M, Kay LM (2016) Gamma and beta oscillations define a sequence of neurocognitive modes present in odor processing. J Neurosci 36:7750–7767. CrossRef Medline

Fries P (2005) A mechanism for cognitive dynamics: neuronal communication through neuronal coherence. Trends Cogn Sci 9:474–480. CrossRef Medline

Garcia AJ 3rd, Zanella S, Koch H, Doi A, Ramirez JM (2011) Chapter 3–networks within networks: the neuronal control of breathing. Prog Brain Res 188:31–50. CrossRef Medline

Haberly LB, Price JL (1978) Association and commissural fiber systems of the olfactory cortex of the rat. J Comp Neurol 178:711–740. CrossRef Medline

Heinemann U, Gabriel S, Jauch R, Schulze K, Kivi A, Eilers A, Kovacs R, Lehmann TN (2000) Alterations of glial cell function in temporal lobe epilepsy. Epilepsia 41 [Suppl 6]:S185–S189. Medline

Hermes D, Miller KJ, Noordmans HJ, Vansteensel MJ, Ramsey NF (2010) Automated electrocorticographic electrode localization on individually rendered brain surfaces. J Neurosci Methods 185:293–298. CrossRef Medline

Hiltunen T, Kantola J, Abou Elseoud A, Lepola P, Suominen K, Starck T, Nikkinen J, Remes J, Tervonen O, Palva S, Kiviniemi V, Palva JM (2014) Infra-slow EEG fluctuations are correlated with resting-state network dynamics in FMRI. J Neurosci 34:356–362. CrossRef Medline

Hudry J, Ryvlin P, Royet JP, Mauguière F (2001) Odorants elicit evoked potentials in the human amygdala. Cereb Cortex 11:619–627. CrossRef Medline

Hughes JR, Andy OJ (1979) The human amygdala. I. Electrophysiological responses to odorants. Electroencephalogr Clin Neurophysiol 46:428–443. CrossRef Medline

Huijbers W, Pennartz CMA, Beldzik E, Domagalik A, Vinck M, Hofman WF, Cabeza R, Daselaar SM (2014) Respiration phase-locks to fast stimulus presentations: implications for the interpretation of posterior midline "deactivations." Hum Brain Mapp 35:4932–4943. CrossRef

Ito J, Roy S, Liu Y, Cao Y, Fletcher M, Lu L, Boughter JD, Grün S, Heck DH (2014) Whisker barrel cortex delta oscillations and gamma power in the awake mouse are linked to respiration. Nat Commun 5:3572. CrossRef Medline

Jensen O, Colgin LL (2007) Cross-frequency coupling between neuronal oscillations. Trends Cogn Sci 11:267–269. CrossRef Medline

Johnson BN, Russell C, Khan RM, Sobel N (2006) A comparison of methods for sniff measurement concurrent with olfactory tasks in humans. Chem Senses 31:795–806. CrossRef Medline

Jung J, Hudry J, Ryvlin P, Royet JP, Bertrand O, Lachaux JP (2006) Functional significance of olfactory-induced oscillations in the human amygdala. Cereb Cortex 16:1–8. CrossRef Medline

Kay LM (2005) Theta oscillations and sensorimotor performance. Proc Natl Acad Sci U S A 102:3863–3868. CrossRef Medline

Kay LM, Beshel J (2010) A beta oscillation network in the rat olfactory sys-

tem during a 2-alternative choice odor discrimination task. J Neurophysiol 104:829–839. CrossRef Medline

Kay LM, Freeman WJ (1998) Bidirectional processing in the olfactory-limbic axis during olfactory behavior. Behav Neurosci 112:541–553. CrossRef Medline

Kepecs A, Uchida N, Mainen ZF (2006) The sniff as a unit of olfactory processing. Chem Senses 31:167–179. CrossRef Medline

Kleinfeld D, Deschênes M, Wang F, Moore JD (2014) More than a rhythm of life: breathing as a binder of orofacial sensation. Nat Neurosci 17:647–651. CrossRef Medline

Kleinfeld D, Deschênes M, Ulanovsky N (2016) Whisking, sniffing, and the hippocampal theta-rhythm: a tale of two oscillators. PLoS Biol 14: e1002385. Medline

Lakatos P, Shah AS, Knuth KH, Ulbert I, Karmos G, Schroeder CE (2005) An oscillatory hierarchy controlling neuronal excitability and stimulus processing in the auditory cortex. J Neurophysiol 94:1904–1911. CrossRef Medline

Laming PR, Kimelberg H, Robinson S, Salm A, Hawrylak N, Müller C, Roots B, Ng K (2000) Neuronal-glial interactions and behaviour. Neurosci Biobehav Rev 24:295–340. CrossRef Medline

Laurent G, Stopfer M, Friedrich RW, Rabinovich MI, Volkovskii A, Abarbanel HD (2001) Odor encoding as an active, dynamical process: experiments, computation, and theory. Annu Rev Neurosci 24:263–297. CrossRef Medline

LeDoux JE (2000) Emotion circuits in the brain. Annu Rev Neurosci 23: 155–184. CrossRef Medline

Li S, Weerda R, Milde C, Wolf OT, Thiel CM (2014) Effects of acute psychosocial stress on neural activity to emotional and neutral faces in a face recognition memory paradigm. Brain Imaging Behav 8:598–610. CrossRef Medline

Lisman JE, Idiart MA (1995) Storage of 7 +/- 2 short-term memories in oscillatory subcycles. Science 267:1512–1515. CrossRef Medline

Lisman JE, Jensen O (2013) The theta-gamma neural code. Neuron 77: 1002–1016. CrossRef Medline

Litaudon P, Garcia S, Buonviso N (2008) Strong coupling between pyramidal cell activity and network oscillations in the olfactory cortex. Neuroscience 156:781–787. CrossRef Medline

Liu CC, Chien JH, Kim JH, Chuang YF, Cheng DT, Anderson WS, Lenz FA (2015) Cross-frequency coupling in deep brain structures upon processing the painful sensory inputs. Neuroscience 303:412–421. CrossRef Medline

Lowry CA, Kay LM (2007) Chemical factors determine olfactory system beta oscillations in waking rats. J Neurophysiol 98:394–404. CrossRef Medline

Macrides F (1975) Temporal relationships between hippocampal slow waves and exploratory sniffing in hamsters. Behav Biol 14:295–308. CrossRef Medline

Macrides F, Eichenbaum HB, Forbes WB (1982) Temporal relationship between sniffing and the limbic theta rhythm during odor discrimination reversal learning. J Neurosci 2:1705–1717. Medline

Mainland J, Sobel N (2006) The sniff is part of the olfactory percept. Chem Senses 31:181–196. CrossRef Medline

Mantini D, Perrucci MG, Del Gratta C, Romani GL, Corbetta M (2007) Electrophysiological signatures of resting state networks in the human brain. Proc Natl Acad Sci U S A 104:13170–13175. CrossRef Medline

Martin C, Ravel N (2014) Beta and gamma oscillatory activities associated with olfactory memory tasks: different rhythms for different functional networks? Front Behav Neurosci 8:218. Medline

Martin C, Beshel J, Kay LM (2007) An olfacto-hippocampal network is dynamically involved in odor-discrimination learning. J Neurophysiol 98: 2196–2205. CrossRef Medline

Moore JD, Deschênes M, Furuta T, Huber D, Smear MC, Demers M, Kleinfeld D (2013) Hierarchy of orofacial rhythms revealed through whisking and breathing. Nature 497:205–210. CrossRef Medline

Moreno-Martínez FJ, Montoro PR (2012) An ecological alternative to snodgrass and vanderwart: 360 high quality colour images with norms for seven psycholinguistic variables. PLoS One 7:e37527. CrossRef Medline

Mormann F, Fell J, Axmacher N, Weber B, Lehnertz K, Elger CE, Fernández G (2005) Phase/amplitude reset and theta-gamma interaction in the human medial temporal lobe during a continuous word recognition memory task. Hippocampus 15:890–900. CrossRef Medline

Neville KR, Haberly LB (2003) Beta and gamma oscillations in the olfactory system of the urethane-anesthetized rat. J Neurophysiol 90:3921–3930. CrossRef Medline

Nguyen Chi V, Müller C, Wolfenstetter T, Yanovsky Y, Draguhn A, Tort AB, Brankačk J (2016) Hippocampal respiration-driven rhythm distinct from theta oscillations in awake mice. J Neurosci 36:162–177. CrossRef Medline

Oostenveld R, Fries P, Maris E, Schoffelen JM (2011) Fieldtrip: open source software for advanced analysis of MEG, EEG, and invasive electrophysiological data. Comput Intell Neurosci 2011:156869. CrossRef Medline

Palva JM, Monto S, Kulashekhar S, Palva S (2010) Neuronal synchrony reveals working memory networks and predicts individual memory capacity. Proc Natl Acad Sci U S A 107:7580–7585. CrossRef Medline

Pelli DG (1997) The videotoolbox software for visual psychophysics: transforming numbers into movies. Spat Vis 10:437–442. CrossRef Medline

Picchioni D, Horovitz SG, Fukunaga M, Carr WS, Meltzer JA, Balkin TJ, Duyn JH, Braun AR (2011) Infraslow EEG oscillations organize large-scale cortical-subcortical interactions during sleep: a combined EEG/FMRI study. Brain Res 1374:63–72. CrossRef Medline

Poo C, Isaacson JS (2009) Odor representations in olfactory cortex: "sparse" coding, global inhibition, and oscillations. Neuron 62:850–861. CrossRef Medline

Ranade S, Hangya B, Kepecs A (2013) Multiple modes of phase locking between sniffing and whisking during active exploration. J Neurosci 33: 8250–8256. CrossRef Medline

Rojas-Líbano D, Frederick DE, Egaña JI, Kay LM (2014) The olfactory bulb theta rhythm follows all frequencies of diaphragmatic respiration in the freely behaving rat. Front Behav Neurosci 8:214. CrossRef Medline

Root CM, Denny CA, Hen R, Axel R (2014) The participation of cortical amygdala in innate, odour-driven behaviour. Nature 515:269–273. CrossRef Medline

Sanchez-Vives MV, Nowak LG, McCormick DA (2000) Cellular mechanisms of long-lasting adaptation in visual cortical neurons *in vitro*. J Neurosci 20:4286–4299. Medline

Schack B, Weiss S (2005) Quantification of phase synchronization phenomena and their importance for verbal memory processes. Biol Cybern 92: 275–287. CrossRef Medline

Schack B, Vath N, Petsche H, Geissler HG, Möller E (2002) Phase-coupling of theta-gamma EEG rhythms during short-term memory processing. Int J Psychophysiol 44:143–163. CrossRef Medline

Sirotin YB, Costa ME, Laplagne DA (2014) Rodent ultrasonic vocalizations are bound to active sniffing behavior. Front Behav Neurosci 8:399. CrossRef Medline

Smith JC, Ellenberger HH, Ballanyi K, Richter DW, Feldman JL (1991) Pre-Botzinger complex: a brainstem region that may generate respiratory rhythm in mammals. Science 254:726–729. CrossRef Medline

Smith JC, Abdala AP, Rybak IA, Paton JF (2009) Structural and functional architecture of respiratory networks in the mammalian brainstem. Philos Trans R Soc Lond B Biol Sci 364:2577–2587. CrossRef Medline

Sobel N, Prabhakaran V, Desmond JE, Glover GH, Goode RL, Sullivan EV, Gabrieli JD (1998) Sniffing and smelling: separate subsystems in the human olfactory cortex. Nature 392:282–286. CrossRef Medline

Suess WM, Alexander AB, Smith DD, Sweeney HW, Marion RJ (1980) The effects of psychological stress on respiration: a preliminary study of anxiety and hyperventilation. Psychophysiology 17:535–540. CrossRef Medline

Szczepanski SM, Crone NE, Kuperman RA, Auguste KI, Parvizi J, Knight RT (2014) Dynamic changes in phase-amplitude coupling facilitate spatial attention control in fronto-parietal cortex. PLoS Biol 12:e1001936. CrossRef Medline

Timofeev I, Grenier F, Bazhenov M, Sejnowski TJ, Steriade M (2000) Origin of slow cortical oscillations in deafferented cortical slabs. Cereb Cortex 10:1185–1199. CrossRef Medline

Tort AB, Kramer MA, Thorn C, Gibson DJ, Kubota Y, Graybiel AM, Kopell NJ (2008) Dynamic cross-frequency couplings of local field potential oscillations in rat striatum and hippocampus during performance of a t-maze task. Proc Natl Acad Sci U S A 105:20517–20522. CrossRef Medline

Tort AB, Komorowski RW, Manns JR, Kopell NJ, Eichenbaum H (2009)

Theta-gamma coupling increases during the learning of item-context associations. Proc Natl Acad Sci U S A 106:20942–20947. CrossRef Medline

Tort AB, Komorowski R, Eichenbaum H, Kopell N (2010) Measuring phase-amplitude coupling between neuronal oscillations of different frequencies. J Neurophysiol 104:1195–1210. CrossRef Medline

Usher M, Cohen JD, Servan-Schreiber D, Rajkowski J, Aston-Jones G (1999) The role of locus coeruleus in the regulation of cognitive performance. Science 283:549–554. CrossRef Medline

Vanhatalo S, Tallgren P, Becker C, Holmes MD, Miller JW, Kaila K, Voipio J (2003) Scalp-recorded slow EEG responses generated in response to hemodynamic changes in the human brain. Clin Neurophysiol 114:1744–1754. CrossRef Medline

Verhagen JV, Wesson DW, Netoff TI, White JA, Wachowiak M (2007) Sniffing controls an adaptive filter of sensory input to the olfactory bulb. Nat Neurosci 10:631–639. CrossRef Medline

Viczko J, Sharma AV, Pagliardini S, Wolansky T, Dickson CT (2014) Lack of respiratory coupling with neocortical and hippocampal slow oscillations. J Neurosci 34:3937–3946. CrossRef Medline

Vlemincx E, Taelman J, De Peuter S, Van Diest I, Van den Bergh O (2011) Sigh rate and respiratory variability during mental load and sustained attention. Psychophysiology 48:117–120. CrossRef Medline

Voipio J, Tallgren P, Heinonen E, Vanhatalo S, Kaila K (2003) Millivolt-scale dc shifts in the human scalp EEG: evidence for a nonneuronal generator. J Neurophysiol 89:2208–2214. Medline

Voytek B, Canolty RT, Shestyuk A, Crone NE, Parvizi J, Knight RT (2010) Shifts in gamma phase-amplitude coupling frequency from theta to alpha over posterior cortex during visual tasks. Front Hum Neurosci 4:191. CrossRef Medline

Weaver KE, Wander JD, Ko AL, Casimo K, Grabowski TJ, Ojemann JG, Darvas F (2016) Directional patterns of cross frequency phase and amplitude coupling within the resting state mimic patterns of FMRI functional connectivity. Neuroimage 128:238–251. CrossRef Medline

Welker WI (1964) Analysis of sniffing of the albino rat. Behavior 22:223–244. CrossRef

Yadav R, Shah AK, Loeb JA, Swamy MN, Agarwal R (2011) A novel unsupervised spike sorting algorithm for intracranial EEG. Conf Proc IEEE Eng Med Biol Soc 2011:7545–7548. CrossRef Medline

Yanovsky Y, Ciatipis M, Draguhn A, Tort AB, Brankačk J (2014) Slow oscillations in the mouse hippocampus entrained by nasal respiration. J Neurosci 34:5949–5964. CrossRef Medline

Ye X, He S, Hu Y, Yu YQ, Wang K (2014) Interference between conscious and unconscious facial expression information. PLoS One 9:e105156. CrossRef Medline